

## Review Article

# Teleseismic tomography of the southern Puna plateau in Argentina and adjacent regions

M. Bianchi <sup>a</sup>, B. Heit <sup>a,\*</sup>, A. Jakovlev <sup>b</sup>, X. Yuan <sup>a</sup>, S.M. Kay <sup>c</sup>, E. Sandvol <sup>d</sup>, R.N. Alonso <sup>e</sup>, B. Coira <sup>f</sup>, L. Brown <sup>c</sup>, R. Kind <sup>a,g</sup>, D. Comte <sup>h</sup>

<sup>a</sup> Deutsches GeoForschungsZentrum GFZ, Telegrafenberg, 14473 Potsdam, Germany

<sup>b</sup> Institute of Geology, SB RAS, Novosibirsk, Russia

<sup>c</sup> Cornell University, EAS, Snee Hall, Ithaca, NY 14850, United States

<sup>d</sup> Department of Geological Sciences, University of Missouri, Columbia, MO 65211, United States

<sup>e</sup> Universidad Nacional de Salta, Buenos Aires 177, 4400-Salta, Argentina

<sup>f</sup> CONICET, Instituto de Geología y Minería, Universidad Nacional de Jujuy, Avda. Bolivia 1661, 4600-San Salvador de Jujuy, Argentina

<sup>g</sup> Freie Universität Berlin, Maltesserstr. 74-100, 12227 Berlin, Germany

<sup>h</sup> Departamento de Geofísica, Universidad de Chile, Santiago, Chile

## ARTICLE INFO

## Article history:

Received 15 May 2012

Received in revised form 7 September 2012

Accepted 19 November 2012

Available online 30 November 2012

## Keywords:

Central Andes

Puna plateau

Teleseismic tomography

Arc and back-arc volcanoes

Velocity anomalies

Lithospheric structure

## ABSTRACT

We performed a teleseismic P wave tomography study using seismic events at both teleseismic and regional distances, recorded by a temporary seismic array in the Argentine Puna Plateau and adjacent regions. The tomographic images show the presence of a number of positive and negative anomalies in a depth range of 20–300 km beneath the array. The most prominent of these anomalies corresponds to a low-velocity body, located in the crust, most clearly seen in the center of the array (27°S, 67°W) between the Cerro Peinado volcano, the Cerro Blanco caldera and the Farallon Negro in the east. This anomaly (southern Puna Magmatic Body) extends from the northern most part of the array and follows the line with the highest density of stations towards the south where it becomes smaller. It is flanked by high velocities on the west and the east respectively. On the west, the high velocities might be related to the subducted Nazca plate. On the northeast the high velocity block coincides with the position of the Hombre Muerto basin in the crust and could be indicating an area of lithospheric delamination where we detected a high velocity block at 100 km depth on the eastern border of the Puna plateau, north of Galan. This block might be related to a delamination event in an area with a thick crust of Paleozoic metamorphic rocks at the border between Puna and Eastern Cordillera. In the center of the array the Southern Puna magmatic body is also flanked by high velocities but the most prominent region is located on the east and is interpreted as part of the Sierras Pampeanas lithosphere with high velocities. The position of the Sierras Pampeanas geological province is key in this area as it appears to limit the extension of the plateau towards the south.

© 2012 Elsevier B.V. All rights reserved.

## Contents

1.	Introduction . . . . .	66
2.	Data and methodology . . . . .	67
2.1.	The seismic network . . . . .	67
2.2.	Data preparation and phase picking . . . . .	67
2.3.	Inversion of teleseismic events . . . . .	69
2.4.	Inversion of regional events . . . . .	70
2.5.	Joint inversion of teleseismic and regional events . . . . .	70
2.6.	Results of the joint inversion . . . . .	71
2.7.	Synthetic resolution tests . . . . .	71
2.8.	Tomographic results and relation to important regional features . . . . .	72
3.	Discussion . . . . .	74

\* Corresponding author. Tel.: +49 3312881860; fax: +49 3312881277.

E-mail address: [heit@gfz-potsdam.de](mailto:heit@gfz-potsdam.de) (B. Heit).

4. Relationship to the delamination model . . . . .	81
5. Conclusions . . . . .	81
Acknowledgements . . . . .	82
References . . . . .	82

## 1. Introduction

The Andean mountains are directly related to the process of subduction of the oceanic Nazca plate beneath the South American continental plate. The main topographic feature in the Central Andes is known as the Altiplano-Puna plateau, which is flanked by regions of sub-horizontally subducting segments to the north and south. The approximate dividing line between the distinctive Puna and Altiplano parts of the plateau is approximately at the latitude of 22°S, near the Bolivian–Argentine border (Fig. 1A). Significant variations along the plateau include local differences in the pre Andean geologic history; Andean uplift, amount of shortening and magmatism, and modern topography and Wadati–Benioff geometry. (e.g., Allmendinger et al., 1997; Cahill and Isacks, 1992; Kay and Coira, 2009; Oncken et al., 2006 and references therein).

In general, the Puna plateau is bounded to the west by the Andean Neogene Central Volcanic Zone (Western Cordillera, WC or Central Volcanic Zone, CVZ) and to the east by an active westward verging thin-skinned foreland thrust belt (deformed Paleozoic rocks of the Eastern Cordillera). Allmendinger et al. (1997) summarize the evidence that the Puna does not present a well-developed thin-skinned thrust belt to the east and has more irregular topography than the Altiplano.

The more irregular topographic surface of the Puna plateau is due to the effects of crustal segmentation that created small closed basins that are responsible for localized shortening and surface uplift at both margins of the plateau (e.g., Riller and Oncken, 2003). Such segmentation is induced, in part, by a number of lineaments or strike-slip faults limiting continuous deformation across the plateau. Some of these lineaments are seismically active (e.g. Schurr et al., 1999), with small earthquakes concentrated along the eastern border of the plateau and the Olacapato-Toro Lineament (known as the Olacapato-El Toro Fault Zone). The Olacapato-Toro Lineament (OT-L) is a prominent shear zone located to the north of our study region which extends northwest from the city of Salta across the Puna plateau and may reach the coast of Chile. A recent magnitude Mw 6.1 earthquake on the 27th February 2010 indicates that this fault system is still tectonically active. These lineaments are considered to play a key role in the differences between the northern and southern Puna plateau (e.g. Alonso et al., 1984; Ramos, 1999) (Fig. 1A).

The northern Puna plateau, between ~22°S and 24.5°S, is structurally separated from the southern Puna, ~25°S–28°S, by the NW–SE-trending lineament (i.e. O–T–L) (Fig. 1A). A system of parallel strike-slip faults to the north and south, which are considered to be zones of lithospheric weakness (i.e. Archibarca, Culampaja and Ojos del Salado lineaments) coincide with a series of strato-volcanic edifices that comprise the largest volcanoes of the Puna plateau and some of the highest active volcanoes on earth (e.g. Ojos del Salado). The most significant north–south structural changes in the back-arc, along the eastern border of the plateau are the termination of the thin-skinned Subandean belt near 23°S. This change correlates with the end of Paleozoic basins and the superposition of the Upper Cretaceous rift basins in the foreland south of 24°S where the thick-skinned Santa Barbara System replaces the thin-skinned Subandean belt and south of 26°S where northern Sierras Pampeanas replace the Eastern Cordillera (Fig. 1B) (e.g., Allmendinger et al., 1997; Kay and Coira, 2009; Kley and Monaldi, 1998).

Topographically, the Puna plateau in Argentina has an average altitude of ~4.2 km above sea level and is about 1 km higher than the Altiplano plateau of Bolivia (~3.2 km). The crustal thickness of the northern Puna plateau is ~60 km (i.e. 10 km thinner than the

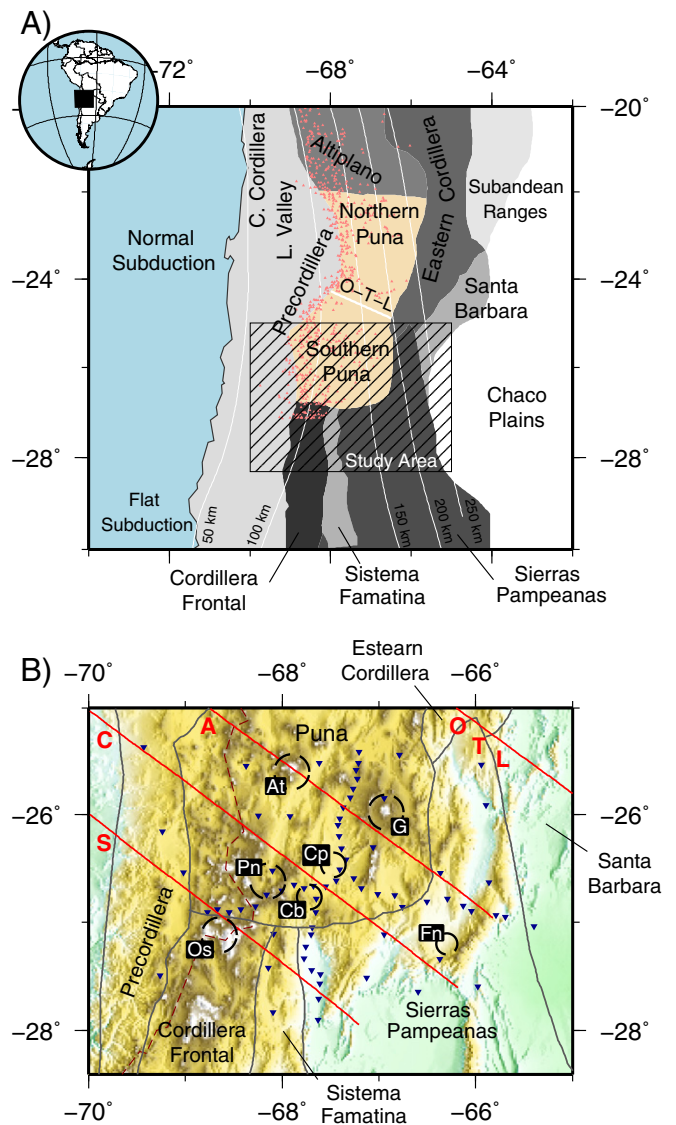


**Fig. 1.** A) Map showing the main tectonic units in the region of the central Andes between 20° and 28°S. Red triangles denote volcanoes. White curves denote contours of the subducted slab (Cahill and Isacks, 1992). B) Map showing the distribution of stations (blue inverted triangles) and the different tectonic units (gray lines) in the southern Puna. The red dashed line is the Chile/Argentina border. The red solid lines are tectonic lineaments (A: Archibarca, C: Culampaja, S: Ojos del Salado, OTL: Olacapato-Toro-Lineament). The major volcanic centers inside the array are marked with black circles; At: Antofalla; G: Cerro Galan Caldera; Cp: Carachi Pampa; Pn: Peinado; Cb: Cerro Blanco Caldera; Os: Ojos del Salado; and Fn: Farallon Negro.

Altiplano) and has a Moho topography with significant depth variations beneath the plateau north of 24°S (e.g. McGlashan et al., 2008; Yuan et al., 2002) and is more homogeneous near 25°S (e.g. Heit et al., 2007; Woelbern et al., 2009). Young mafic magmatism in the southern part of the Puna has been described as one of the important features distinguishing the northern and southern parts of the plateau (Kay et al., 1994). These observations have also been used as evidence of more recent delamination of a part of the lower crust and upper mantle to explain the higher topography and thinner lithosphere under the southern Puna (e.g. Kay and Kay, 1993; Kay et al., 1994; Whitman et al., 1996).

The Southern Puna plateau has a thinner continental lithosphere (Heit et al., 2007; Whitman et al., 1992), a slab with an intermediate dip between a steeper segment to the north and a shallower segment to the south (e.g., Cahill and Isacks, 1992; Mulcahy, 2012; Mulcahy et al., 2010 in prep) and a distinct sedimentary and magmatic and structural history (e.g. Allmendinger et al., 1997; Coira et al., 1993; Kay and Coira, 2009; Kay et al., 1999; Marrett et al., 1994) than the Altiplano. Furthermore, the estimated crustal shortening ratio is less in the region of the Puna than the Altiplano (e.g. Kley and Monaldi, 1998; Kley et al., 1999) and is concentrated in the Eastern Cordillera, the Santa Barbara System and the northern end of the Pampean ranges.

Francis et al. (1989) De Silva and Gosnold (2007) and Kay et al. (2010, 2011a) among others have discussed the amount and generation of crustal melts in the Puna plateau and all interpret the large-volume ignimbrites as having at least 50% crustal melt. Kay and Kay (1993) and Kay et al. (1994) Kay et al. (2011a, 2011b) have suggested that the presence of the ~6.5–2 Ma Cerro Galan caldera and its sequence of associated large ignimbrite deposits are a consequence of delamination processes in the southern Puna.

The differences in compositions of the volcanic rocks in the southern Puna may reflect the characteristics of the mantle derived fluids and melts involved in upper-crustal melting (Kay et al., 1994). Schurr et al. (1999, 2003) proposed a model, based on local tomography data, for the Puna at ~24°S where the ascending path for the fluids causes melting of the overlying mantle and suggested a strong horizontal component for the path the magma has taken to the surface.

The Puna south of 25.5°S is a region that prior to this study, had little geophysical information. A thinner lithosphere in the Puna near 25°S was suggested by shear wave attenuation data (Whitman et al., 1992, 1996), gravity interpretations (Prezzi et al., 2009; Tassara et al., 2006) and receiver function estimates by Heit et al. (2007). Gravity measurements also suggest a relatively thin crust under parts of the southern Puna plateau (e.g. Prezzi et al., 2009; Tassara et al., 2006) and are consistent with the crustal thickness values between 45 km and 60 km obtained from seismic data (e.g. McGlashan et al., 2008; Yuan et al., 2002).

Previous seismological studies revealed low velocities in the crust and asthenosphere beneath the southern Puna plateau, suggesting higher temperatures than the northern Puna and the Altiplano (Heit, 2005; Heit et al., 2007, 2008; Isacks, 1988; Scire et al., 2011; Whitman et al., 1992, 1996; Woelbern et al., 2009). The maximum crustal thickness along a profile at 25.5°S obtained from the receiver function image, is nearly 60 km and the tomographic images show low velocity anomalies in the crust that lessen into the mantle indicating that are consistent with asthenospheric material reaching the Moho (Heit, 2005; Woelbern et al., 2009).

From November 2007 to October 2009 a passive source seismic experiment was deployed throughout the southern Puna plateau between 25°S and 28°S by US, German, Argentine and Chilean institutions (see Fig. 1B). Travel time data from this array are used in this study to resolve more clearly the subsurface structure beneath the southern Puna by performing an integrated tomographic analysis using teleseismic and regional events.

## 2. Data and methodology

### 2.1. The seismic network

A passive source seismic array, of 74 stations, was deployed across the southern Puna Plateau for a period of two years. The station distribution is shown in Fig. 1B. The seismic experiment was configured to have two orthogonal arrays surrounded by a 2D sparse array. The station spacing was between 10 and 20 km along both the north–south and east–west transects while the inter-station distance in the 2D network was 35–50 km. A variety of broadband and intermediate-period sensors were used in the experiment, including Streckeisen STS-2; Güralp 3-T, 3ESP and 40-T; Nanometrics Trillium-40S and Trillium 120S and Mark L4. Continuous waveform data are archived at the IRIS and GEOFON data centers.

### 2.2. Data preparation and phase picking

We performed teleseismic P wave tomography using teleseismic P (including Pdiff) as well as regional P waves. The use of different P waves may help to increase the spatial resolution because of the differences in the ray paths. The regional P waves arrive at shallower incident angles than the teleseismic P wave, whereas the Pdiff waves arrive at the stations at near-vertical incident angles. From the USGS global PDE catalog we selected teleseismic P phases at epicentral distances between 30° and 95° with magnitudes (mb) greater than 5.5; Pdiff at distances of 95°–150° with magnitudes greater than 6.5 and regional P phase between 2° and 30° with magnitudes greater than 5.0. Vertical component waveform data are visually selected for the signal/noise ratio and number of records for each event. The 378 selected events are shown in Fig. 2. The regional events are mainly located along the Andean subduction zone and have a back-azimuth around 0° or 180° in relation to our network. The teleseismic events have a fairly good azimuthal distribution with respect to our network. In total, 17410 ray paths were obtained for the selected events covering the major part of the area with crossing rays beneath the seismic array down to a depth of 300 km as shown in Fig. 3. We

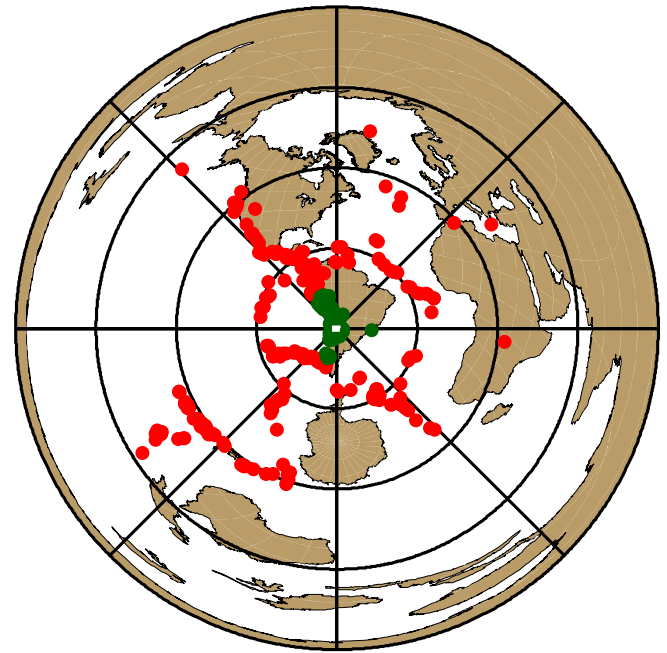
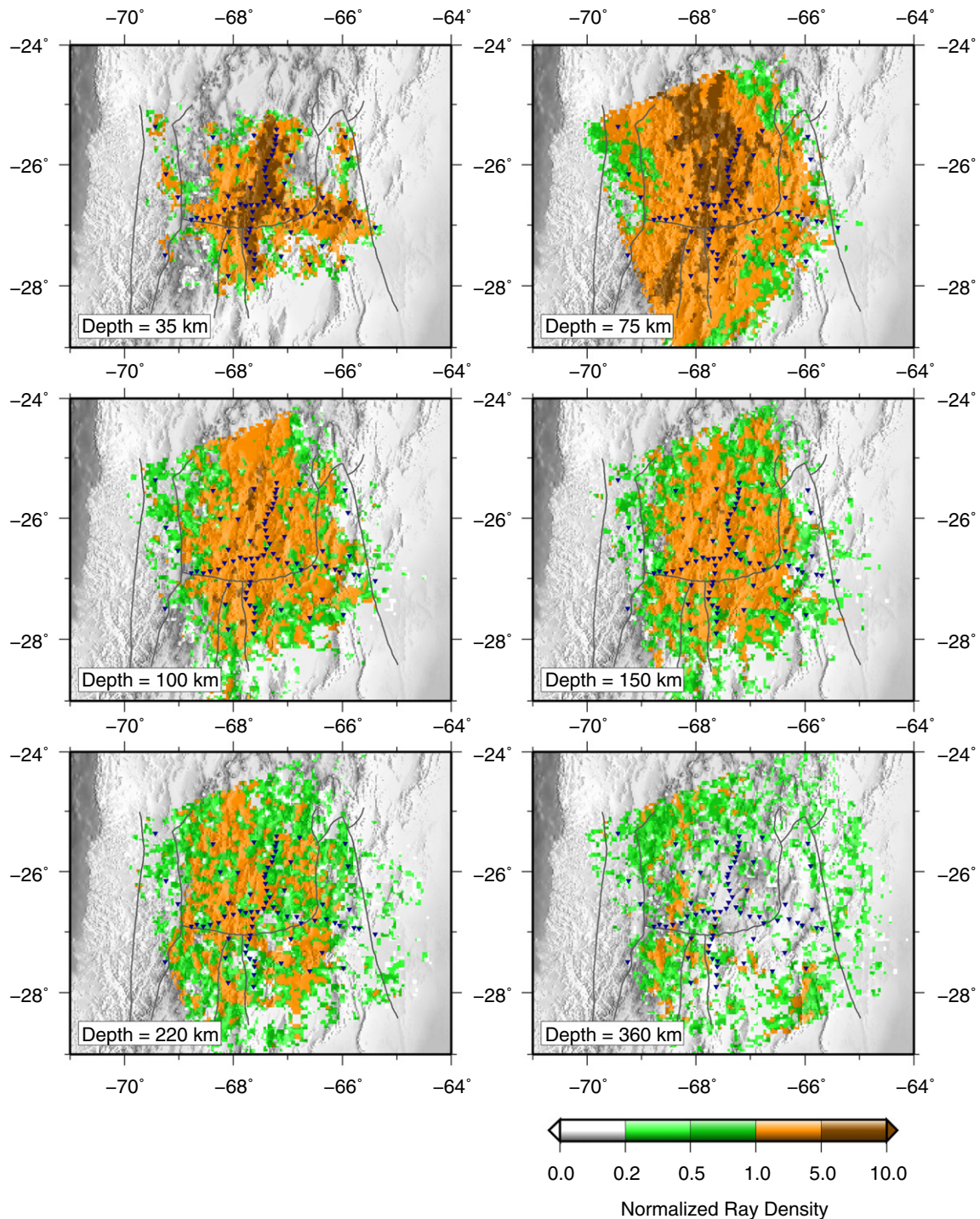


Fig. 2. Map of the teleseismic (red) and regional (green) events used in the inversion. Only those events that have more than 5 picks are considered for the tomographic inversion.



**Fig. 3.** Normalized ray path density at different depths. The ray density was calculated in a regular grid of  $10 \times 10 \times 5$  km. Inside each box instead of counting the number of crossing rays, the total length of the ray segments length is summed up and normalized by the average ray path length per box in our model (42.9 km). A value of 1 means that approximately 4 full ray paths pass through the box, which should indicate good ray coverage. Values smaller than 1 show areas with less than the average ray density. The best ray coverage is located in the lower crust and uppermost mantle at depths of 35–200 km. Solid lines define the major tectonic units as in Fig. 1.

divided the study area by regular grids with the size of  $10 \times 10 \times 5$  km. The normalized ray path density in Fig. 3 represents the length of the total ray paths crossing each box normalized by the average ray path length over the entire model grids with non-zero path length (42.9 km). The best ray coverage is in the lower crust and upper mantle at depths of 35–200 km.

To compare waveforms recorded at different stations with different types of seismometers, we removed the instrument response

from the waveforms and then applied a bandpass filter (0.5 to 2 Hz). For each event, we aligned P waveforms of different stations at the maximum or minimum amplitude and picked the P wave travel time residuals relative to a reference station. In Fig. 4 we show two examples for teleseismic and regional events. In both sections band passed filtered P wave seismograms are sorted by the epicentral distance and aligned by picked P wave arrivals. Theoretical arrival times predicted by the IASP91 model are indicated by the red dots. Seismograms of

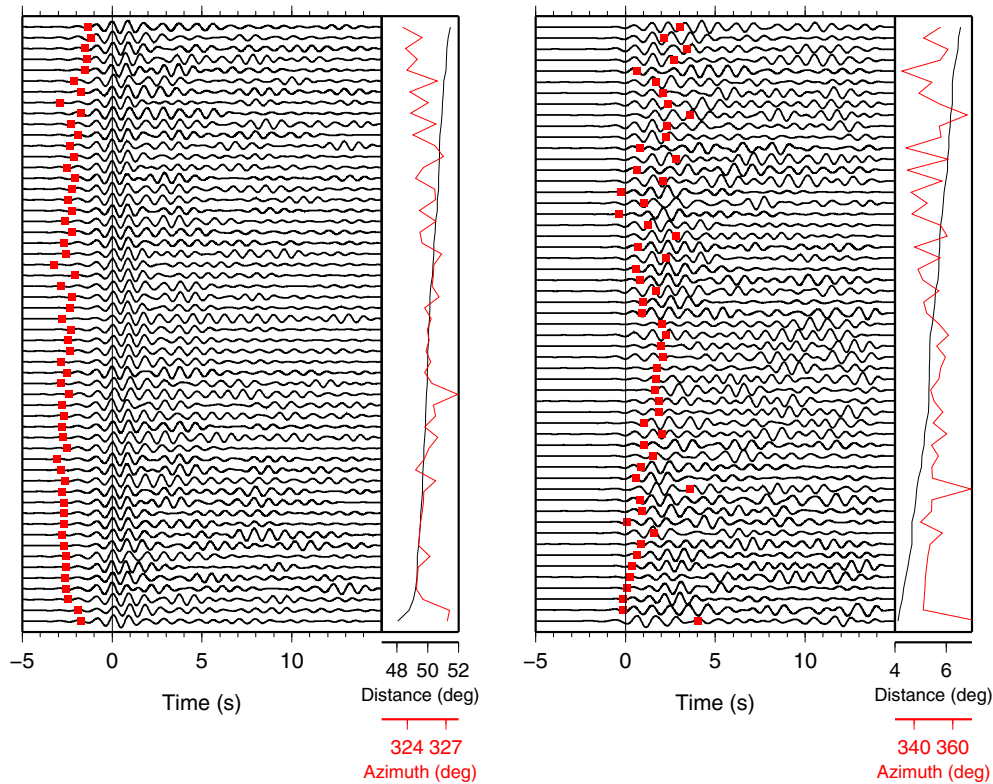


**Fig. 4.** Waveform examples of a teleseismic event (left panel) and a regional event (right panel). Traces are sorted by epicentral distance and aligned by picked P phases. Red dots are theoretical arrivals predicted by the IASP91 model. Epicentral distances and back azimuths are indicated on the right side of each panel. Amplitudes are normalized for individual traces within the display window.

the teleseismic events are very similar, so all the traces are aligned coherently. The wavefield of the regional event displays a complex pattern due to strong heterogeneities along the ray paths and multiple interferences of regional wave fields, such as Pg, Pn and mantle P waves. However, as we picked relative residuals of the regional phases at different stations and the radius of our array is relatively small compared to the majority of the regional path lengths, most regional sections are dominated by the same phases. In the case that multiple phases exist in a section we attempted to pick the earliest arrival. Accordingly, our tomography code uses the first arrival of the regional phases. Therefore, the interference caused by the regional P wave phases is negligible in our inversion. We note that the large residuals at some stations are outliers caused by GPS timing errors due to e.g. poor satellite coverage and are removed from the final dataset.

Station elevation and Moho topography can strongly influence the P wave residuals and should, therefore, be considered while constructing the velocity model. We have collected the Moho depth data from published sources (Heit et al., 2007; McGlashan et al., 2008; Woelbern et al., 2009; Yuan et al., 2002) and created a crustal thickness model after interpolation and smoothing (Fig. 5). We also included some preliminary P and S receiver function results from our own unpublished data using the same dataset to improve the Moho topography.

### 2.3. Inversion of teleseismic events

We followed the approach used by Koulakov and Sobolev (2006) and Heit et al. (2008) and introduced modifications mainly regarding the intrinsic incompatibility of the ray geometry and travel time residuals for regional and teleseismic distance events. The resulting velocity model was computed at the nodes of a parameterization grid distributed in the study volume according to the ray density.

The parameterization nodes are distributed in space according to the ray density (Koulakov, 2009) where the minimum distance between grid nodes is set to 10 km in each direction. We use the same smoothing and damping parameters in all real and synthetic models.

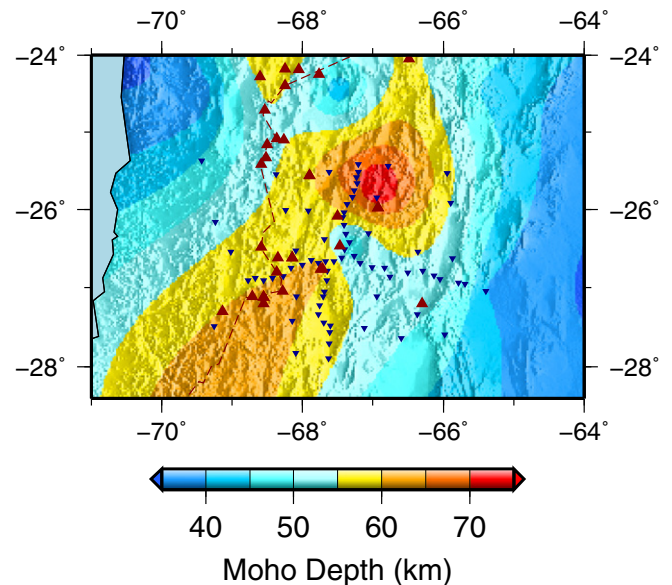


**Fig. 5.** Moho thickness map used for crustal thickness corrections during the inversion process. This map was interpolated using published receiver function results from different authors and part of preliminary measurements by receiver functions from this experiment. The blue inverted triangles denote the position of stations used in the present study. The red triangles are volcanoes.

Therefore, the influence of the chosen values for those parameters can be estimated on the base of the results obtained from the synthetic tests. Our algorithm can be visualized by the flow chart in Fig. 6. In this new approach, we consider both regional and teleseismic data and try to improve the results obtained by these methods independently. By integrating both data sets, we are able to obtain well constrained images from the study area between 20 km and 350 km depth.

The result of the inversion of teleseismic events including only P phases (inversion path *a* in Fig. 6) is shown in Fig. 7. Horizontal sections at depths of 35 and 75 km show widespread low velocities in the crust and uppermost mantle beneath the high Puna Plateau. The Puna plateau can be clearly identified by the distinct borders between low crustal velocities below the plateau and high velocities to the west and southeast of the plateau. The mantle portion at 150 km depth is dominated by the high velocity subducted oceanic slab. Although, it is very difficult to quantify the velocity anomaly of the slab by teleseismic residuals data alone. At 300 km depth, low velocity is widespread in the central area in the mantle beneath the subducted slab, whereas the high velocity anomaly in the eastern part indicates the deeper part of the slab. Note that the extremely high velocity in the southeast corner is, to a certain degree, an artifact, probably caused by the projection of high velocity of the deeper slab outside the study area where the teleseismic rays pass through. As most of the ray paths are near-vertical, there is significant vertical smearing.

#### 2.4. Inversion of regional events

South America is a seismically active region with a high number of earthquakes at local and regional distances from our array. The regional P waves traveling along much shallower paths, can potentially improve the resolution where teleseismic data does not provide any

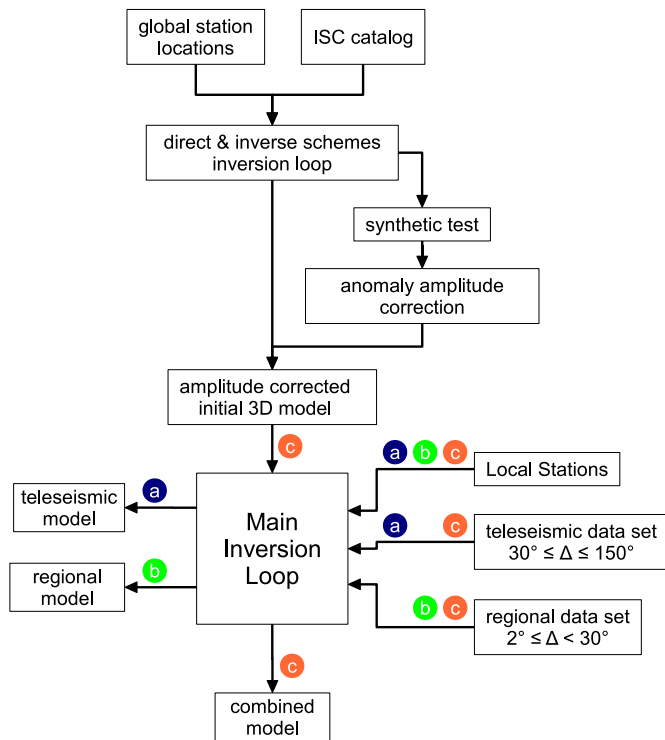


**Fig. 6.** Flow chart showing the different steps and input data used to perform the final inversion. The inversion path (c) is the joint inversion of the teleseismic and regional events, leading to our final (and preferred) model. Paths (a) and (b) show the separate inversions using teleseismic and regional events, respectively.

data. The inclusion of regional events has helped us to increase data coverage, improve the resolution in the crust and resolve some ambiguities caused by vertical smearing. The result of inversion using only regional events (following the inversion path *b* in Fig. 6) can be seen in Fig. 8. These images show the strong influence of the slab as most of the events are located just above the subducting slab between the Nazca and South American plates and have north-south back azimuths. Due to the shallow travel paths, the resolution using only local and regional events, is lost beneath 200 km. Although, some features can be still recognized from the teleseismic only inversion. As in the northeastern corner of our study area; however, the western area has extremely high velocities, which is not seen in the teleseismic inversion in Fig. 7. One explanation for this situation could be that the regional P waves travel parallel to the strike of the subducted Nazca slab so that the travel time residuals might be significantly contaminated by the portion of the high velocity slab outside the study area. This is more evident towards the west where the slab is deepening with a very low angle.

#### 2.5. Joint inversion of teleseismic and regional events

Here we present a joint inversion approach described in Fig. 6 (path *c*) to account for the high velocity anomaly of the slab outside the study area. Based on the International Seismological Center (ISC) earthquake catalog, we performed a global P teleseismic wave tomography focusing on South America to resolve a 3-D structure of the subducted oceanic slab. The joint inversion has resulted in an improved vertical resolution as well as the reduction of apparent slab artifacts.

In this case, we used the data from the ISC in the period from 1964 to 2007, which contains global arrival times recorded at stations of the global seismological network (Fig. 9). The concept of reciprocity of source-receiver pairs can then be used to improve the results in our study area following the approach of Koulakov and Sobolev (2006). They showed that the ITS (Inverse Tomographic Scheme) can produce stable seismic images in regions where seismic sources are located and vice versa considering the position of the stations. Furthermore, the ITS allows the relocation of events simultaneously with the determination of velocity perturbations in one inversion. This simultaneous inversion for source parameters and velocity models should improve the reliability and resolution of the resulting models. In this way, the ITS approach makes use of seismic events in the study region and treats them in a similar way as if they were seismic stations. These events are relocated during the inversion process. It should be noted that the presence of stations within the study region, as in our case, significantly increases the stability of the solution as this allows us to better locate the events.

As in Koulakov and Sobolev (2006), the inversion was performed in several mutually overlapping circular regions, which were later unified into one model. We used a total of six circles located along the axis of the Andes (Fig. 9). The radius of the circles is 8°. The inversion is carried out in fragments because the optimal operation of the ITS is provided when the lateral size of the study region is approximately two times greater than the vertical size. We selected a total of about 13,700 sources located in these circular regions. During their selection, the minimal number of phases was equal to 10 and the minimal empty azimuthal segment did not exceed 180°. A total of 1,160,000 P-phases were selected for the tomographic inversion.

The result of the global tomography using data from the ISC catalog is shown in Fig. 10. Due to an uneven distribution of station and events, the oceanic slab is very well reconstructed in some regions (e.g., lines 1–3), but only partly resolved in others (e.g., lines 4). Line 3 runs across the study area and is relatively well recovered while line 4 covers the area where the flat slab region is located. There are also differences in the parameterization, smoothing and

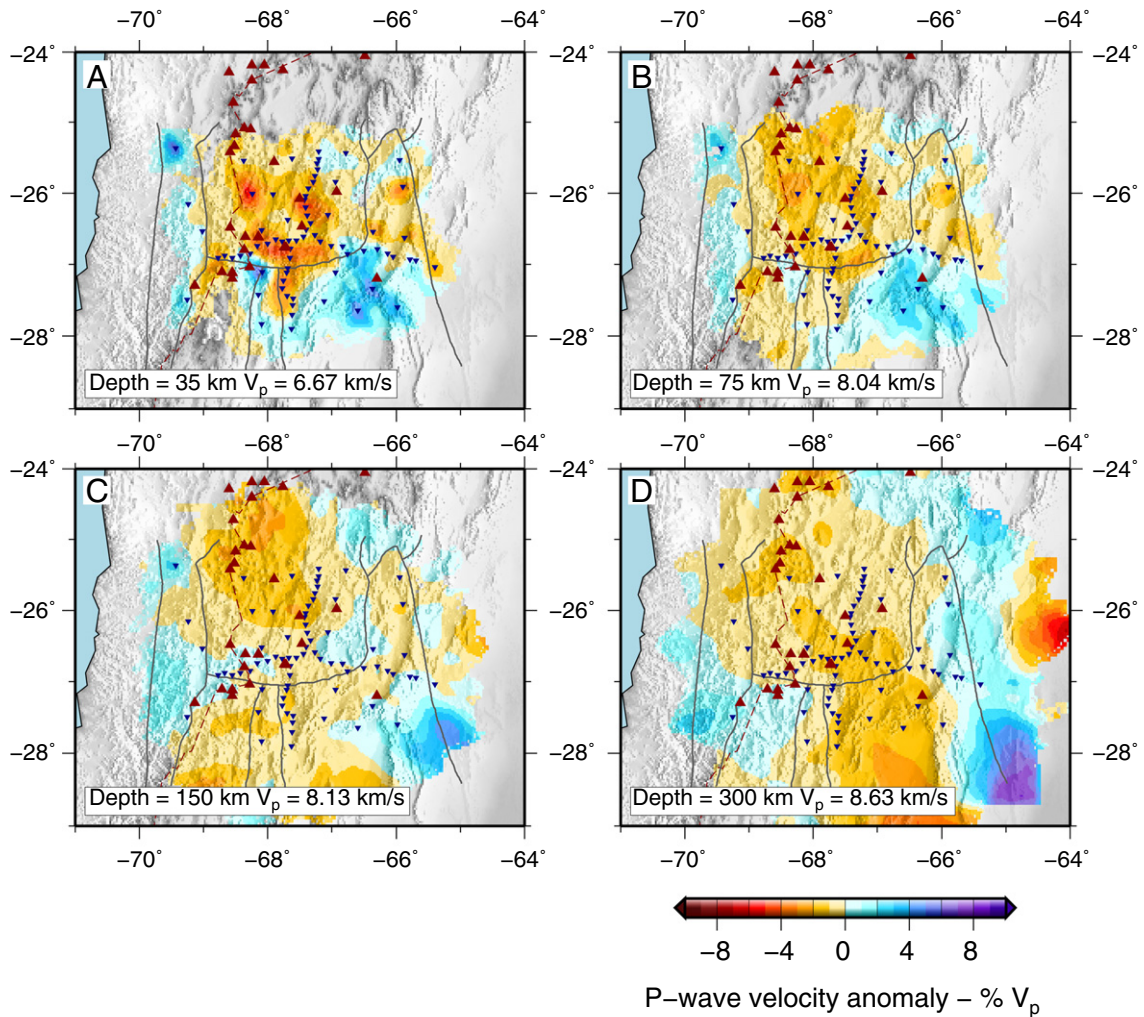


**Fig. 7.** Horizontal sections obtained from the teleseismic inversion following the inversion path (a) in Fig. 6. Red triangles are volcanoes. Stations are denoted by blue inverted triangles. Solid lines define the major tectonic units.

damping between global and regional tomography. To account for these differences, we performed a checkerboard test (the model has +3% and –3% velocity anomalies) for slab resolution by the global inversion and used the result of the test as a guideline to calibrate the slab anomaly for the global inversion. Specifically, we divided the South American continent into several sub-regions and applied the different correction factors obtained in the resolution test to the velocity anomalies for different regions (Fig. 11). We then used the resulting 3-D velocities anomalies obtained below a depth of 80 km as an input model to the tomographic inversion of the P wave residuals from both the teleseismic and regional events. In this way, we performed a joint tomography of the global and regional P waves.

## 2.6. Results of the joint inversion

The final results of the joint inversion are displayed in horizontal sections (Fig. 12) at different depths and in vertical sections (Fig. 13) across and along the strike of the subduction zone. These sections highlight the variations of the anomalies beneath the Puna plateau. We have reasonably good resolution down to a depth of 300 km. Below this depth, the anomalies start to show smearing that tends to increase with depth. Throughout the vertical sections in Fig. 13, the subducted oceanic lithosphere of the Nazca plate is clearly visible as a high velocity anomaly. Being in a transition zone

from normal to flat subduction, the slab shallows from north to south by ~100 km (section E). Widespread crustal low velocity zones in the backarc regions (between 200 and 300 km in section B and between 100 and 300 km in section E) coincide with location of the backarc volcanoes. The strong low velocity zone in the north immediately above the slab (300–400 km in section E) is consistent with earlier seismic tomography studies, in which it was interpreted as an effect of hydration of mantle wedge (Heit, 2005; Schurr et al., 2003). The slab in Fig. 13A seems to be divided by a low velocity anomaly that might originate from fluids released in relation to the clusters of events in the Benioff zone as seen in the north of the array. The resolution of this feature is not well constrained. This low velocity anomaly in the crust might be smeared downwards producing this effect on the slab. There are also some high velocity anomalies in the upper mantle. At shallower levels in the crust, the distribution of low velocity anomalies seems to be concentrated close to young volcanic centers such as the mafic volcanic centers seen southwest and west of Cerro Galan (Fig. 12A).

## 2.7. Synthetic resolution tests

A series of synthetic tests were performed to explore the vertical and horizontal resolutions and to provide essential information about the reliability of the features in the final inversion of the real data.

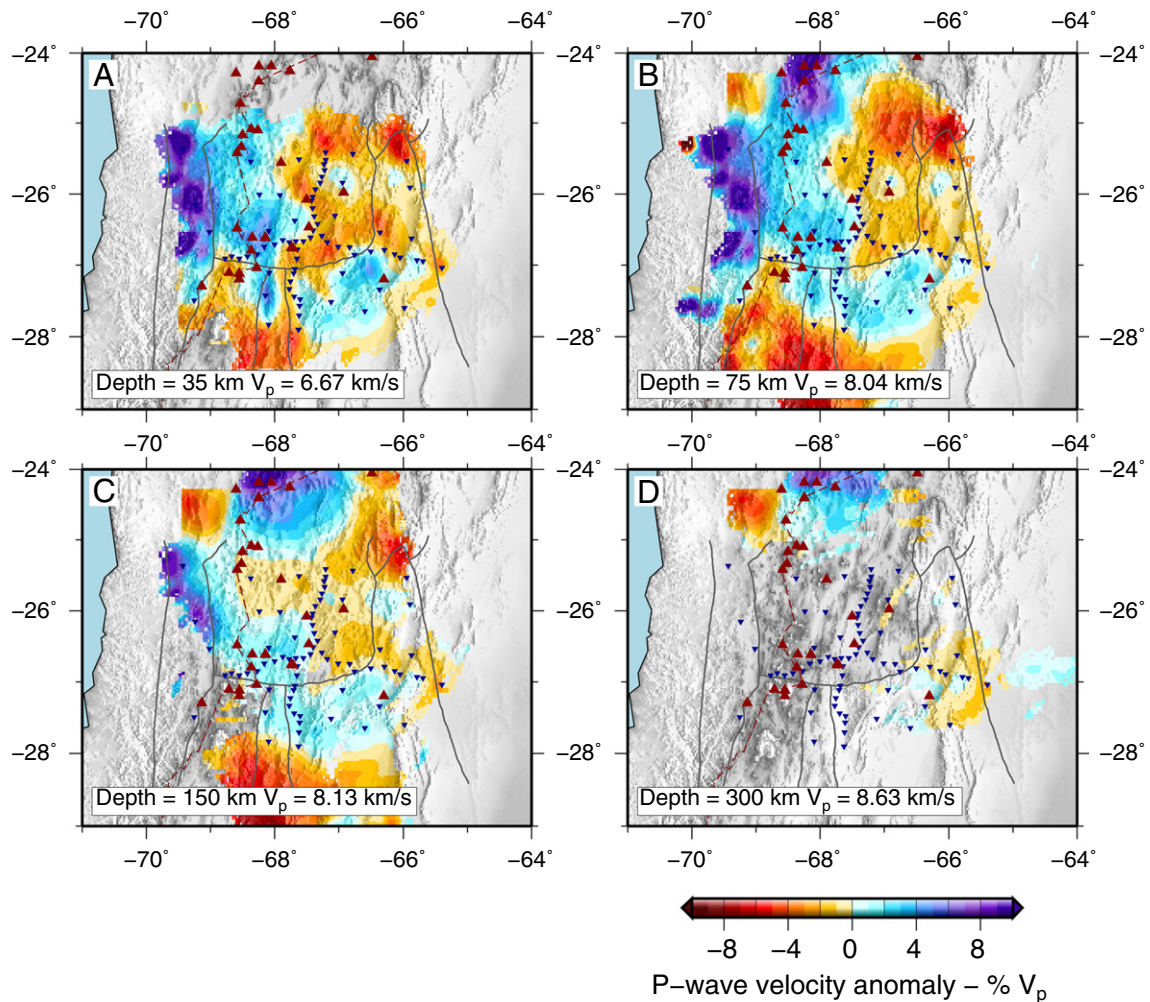


**Fig. 8.** Horizontal sections obtained for the regional inversion following the inversion path (b) in Fig. 6. Red triangles are volcanoes. Stations are denoted by blue inverted triangles. Solid lines define the major tectonic units.

Synthetic tests also provided means to estimate the parameters used in the inversion of the real data. In addition to the checkerboard test (Fig. 14), we also performed the hypothesis tests shown in Fig. 15 (e.g. intra-crustal, lithospheric features and the slab). For all synthetic tests, we use the same geometry (earthquake/stations) as in the case of the real data set.

The checkerboard test is designed to use alternating high and low velocity bodies with sizes of  $100 \times 100 \times 100$  km and  $\pm 3\%$  velocity perturbations (Fig. 14). Random noise (5%) is added to the model. The horizontal synthetic test shows that the position of the anomalies can be well reconstructed from depths of 20 km down to a depth of 290 km in the center of the array, but their shapes become less clear at the border of the array and are therefore not well defined due to smearing. Below 150 km depth the checkerboard test reveals significant smearing in the NW–SE direction due to the dominant orientation of the ray paths from these azimuths. Although, in general, we were able to resolve the synthetic anomalies with minimal smearing.

Vertical sections along the profile lines B and E (i.e. West–East and South–North from Fig. 13) show that the lateral distribution of anomalies and their shape can be reconstructed down to a depth of 300 km.

Additionally some tests based on observed anomalies in the area of the Puna array for regional and teleseismic waves have been performed. The initial anomalies shown in Fig. 15 include three

lithospheric anomalies that represent a low-velocity block ( $-4\%$ ) in the volcanic arc, a high-velocity block of the Puna in the center ( $+4\%$ ), and a low-velocity block in the east which models the eastern border of the plateau ( $-3\%$ ). Both low-velocity blocks can be traced down to 100 km depth, whereas the high velocity block can be traced down to a depth of 150 km. The oceanic slab is represented by the dipping high velocity body ( $+4\%$ ). The residual times for these tests are computed along the real ray paths. The noise is produced by a random number generator, which provides a statistical distribution similar to that of the observed residuals with a predefined synthetic amplitude.

Results of both tests show that the position and shape of the anomalies above and below the slab are well recovered and that only a little smearing occurs in the vertical direction. However, the slab itself completely disappears in the first test verifying that subducted slabs cannot be resolved by using teleseismic data alone in our network nor using data above them (e.g., Evans and Achauer, 1993). The global tomography on the other hand, helps to reconstruct the slab as shown in the same figure (Test 2).

### 2.8. Tomographic results and relation to important regional features

All crustal anomalies are probably influenced by, or related to, the different morpho-structural units that limit the Puna plateau. These include, the volcanic arc known as the Central Volcanic Zone (CVZ)



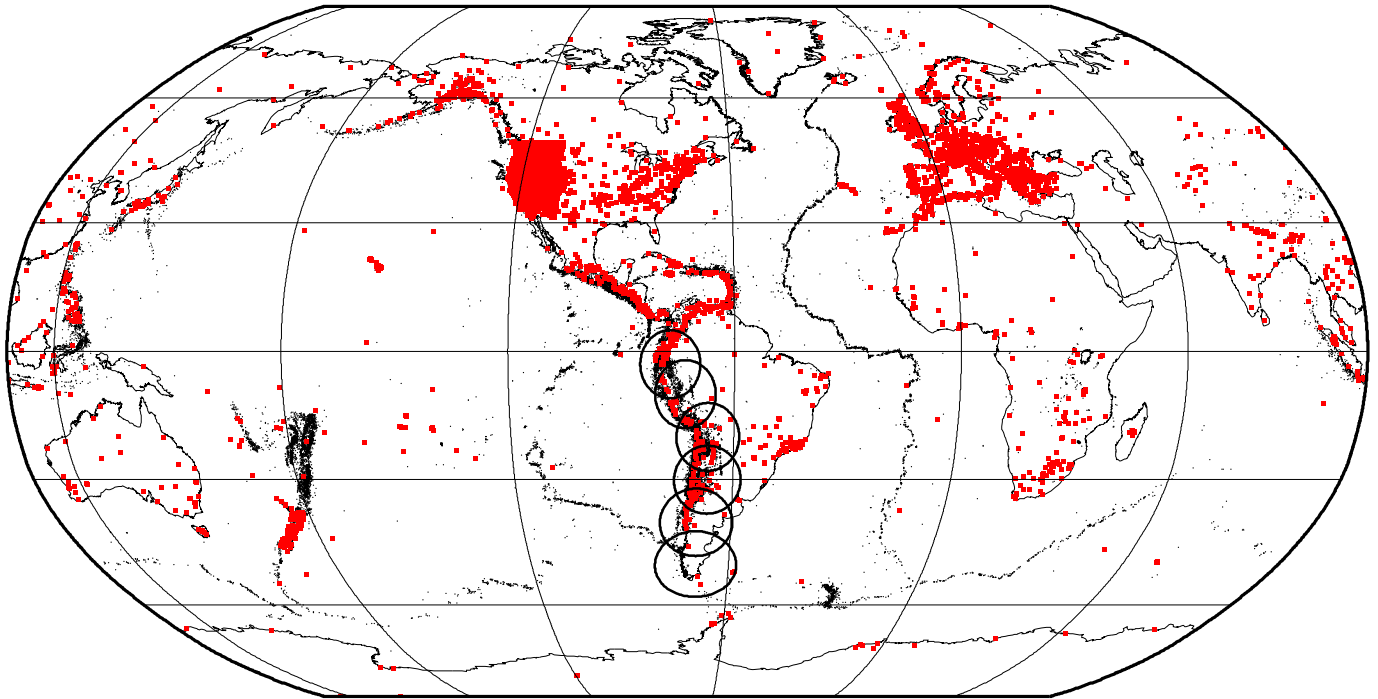


**Fig. 9.** Global distribution of events (black dots) and stations (red dots) used in the inversion of the ISC catalog. The inversion is done simultaneously for direct and inverse schemes. In the direct scheme the inversion is performed using the global events with the South America stations. In the inverse scheme, the events in South America are inverted with the global stations.

on the west and the Eastern Cordillera (EC) (at  $\sim 66^\circ\text{W}$ ), which is bounded by the northern end of the Pampean Ranges to the south and the Santa Barbara System to the east (see Fig. 1). To better estimate the distribution of velocities and their relationships with the position of the different geological units in the area of the array we present the results of tomographic inversion for one horizontal section at a depth of 35 km. The role of magmatic activity, the distribution of certain velocity anomalies and the position of different tectonic units seem to correlate well.

This horizontal tomographic slice at 35 km, which is presented in Fig. 16, shows a clear high velocity region in the west (i.e. blue anomaly west of  $69.5^\circ\text{W}$ ) that corresponds to the zone of interaction between the continental South American and oceanic Nazca plates. East of  $68^\circ\text{W}$ , the velocities tend to be slower and reflect crustal anomalies in a region where estimated crustal thicknesses are around 60 km as seen in Fig. 5 (work in progress; Heit et al., 2010). In the center of the array near  $68^\circ\text{W}$  longitude, this low velocity zone appears to be stronger and correlates with a zone of north–south trending anomalies of similar magnitude that runs from  $\sim 25^\circ\text{S}$  in the north to almost  $28^\circ\text{S}$  in the south. This is the most prominent low velocity anomaly in the southern Puna array and we will discuss in more detail in the next section (see Discussion). From the synthetic tests (Figs. 14 and 15), we know these anomalies should be reliable. Around  $67^\circ\text{W}$  and  $25.5^\circ\text{S}$ , a high velocity block is observed north of the Cerro Galan caldera (feature G). Between  $67^\circ\text{W}$  and  $65^\circ\text{W}$  the most striking feature is the presence of a high velocity block (beneath feature *Fn*) at the southern end of the Puna Plateau (south of  $27^\circ\text{S}$ ) that correlates well with the position of a Precambrian cratonic unit called the Pampean Terrane (e.g. Ramos et al., 1986 and references therein) that is supposed to be the crystalline basement of the Sierras Pampeanas. Two areas of low velocities seem to be independently distributed between  $25^\circ\text{S}$  and  $27^\circ\text{S}$ . Most of the low velocity anomalies described here correlate well with regions of young mafic volcanism and might be said to be controlled by NW–SE trending tectonic lineaments (e.g. Alonso et al., 1984).

Young volcanic arc centers (e.g. Ojos del Salado, Tres Cruces) and backarc calderas (Cerro Galan, Cerro Blanco) are located above low velocity anomalies in the crust, some of which may originate in the upper mantle.

Fig. 16 shows the locations of the major volcanic centers in the region which are included in the discussion below. One of these is the Antofalla volcanic complex (*At* on Fig. 16), which is representative of a group of stratovolcanoes where eruptions began around 14–12 Ma and peaked at 9–8 Ma with satellite cones erupting mafic lavas principally after 7 Ma and mafic flows and small silicic eruptions continuing into the Pleistocene (1.6 Ma) (e.g., Coira and Pezzutti, 1976; Coira et al., 1993; Richards et al., 2006). The young eruptions are linked with an important group of mafic volcanic centers that essentially follows the line of low velocity anomalies starting in the north from the region of the Salar de Hombre Muerto around  $67^\circ\text{W}$  and  $25.5^\circ\text{S}$  to the Cerro Blanco region (*Cb* in Fig. 16) near  $67^\circ\text{S}$  and  $27^\circ\text{S}$ . One of these centers is the Carachi Pampa flow (*Cp* in Fig. 16). Risse et al. (2008) reviewed and presented Ar/Ar ages for the mafic centers showing that this volcanism began at about 6.7–7 Ma and remained focused in the region between Salar de Antofalla and the Cerro Galan caldera, where it is structurally controlled by the juxtaposition of local faults with a mix of compressional, extensional and strike slip motion (e.g., Marrett et al., 1994). Our tomographic images show a good correlation between the distribution of low velocity anomalies and the position of these young mafic volcanic centers.

The largest volcanic center in the region is the giant Cerro Galan ignimbrite caldera complex (*G* on Fig. 16) where eruptions began at about 6 Ma (Sparks et al., 1985) and whose last major eruption is dated at 2.06 Ma (Kay et al., 2011a). These eruptions are postulated to be related to crustal and mantle lithospheric delamination events that led to decompression melting in the mantle producing the basaltic melts that triggered the crustal melting producing the hybrid magmas that erupted to produce these ignimbrites (e.g., Kay et al., 1994, 1999, 2011a). Exactly beneath Cerro Galan there is no significant seismic anomaly (Fig. 16). However, adjacent to it from the north beneath

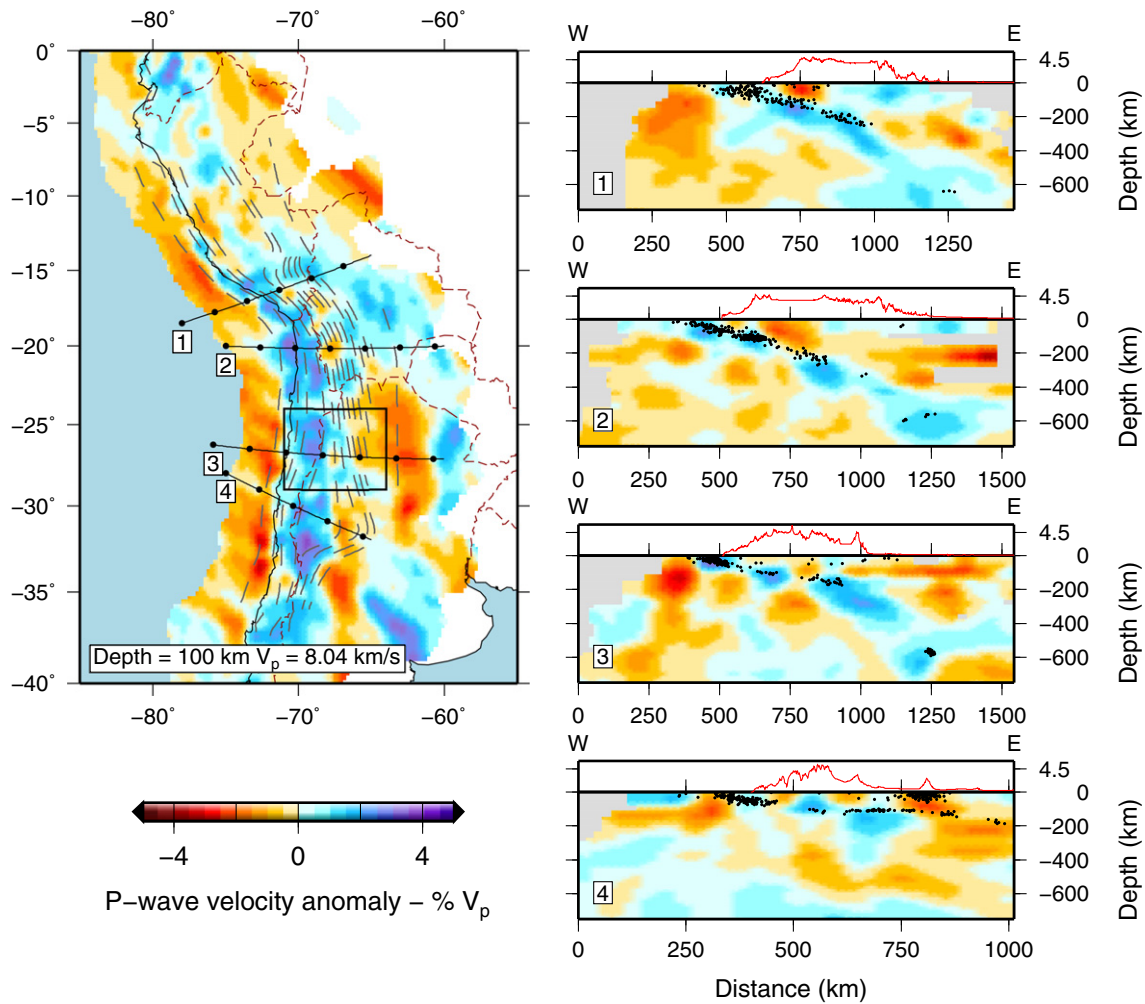


**Fig. 10.** Tomographic inversion results from the ISC catalog using the data shown in Fig. 9. This model is used as a constraint for depths below 80 km in the joint inversion. (Left) Horizontal section representing a tomographic slice at 100 km depth and the position of the study area (black square). The black dots on the profile lines are marks at 250 km horizontal distance. (Right) Different vertical sections from north (1) to south (4). On the cross-sections the black circles are earthquakes. The red line is the topography along each cross-section.

Salar de Hombre Muerto a high-velocity body can be clearly observed in the crust and is named HMB (see Fig. 17).

To the south, young backarc volcanic activity is related to the Peinado volcano (*Pn* on Fig. 16) and the Cerro Blanco volcanic caldera (*Cb* on Fig. 16), in an area that appears to be structurally controlled by the Culampaja lineament. Further south, volcanic activity diminishes drastically, with the youngest activity related to the CVZ Ojos del Salado and Tres Cruces centers (*Os* on Fig. 16). We observed low-velocity anomalies in the crust beneath or in the close vicinity of these volcanic centers.

Beneath the crust at 75 km depth (as seen in Fig. 12), the low velocities are observed only to the northeast and southwest of the array. The strongest low velocity anomaly is located in the northeast approaching the region of the Tuzgle volcano (marked as a reference for this anomaly on Fig. 13) but this is outside our array and we lack of sufficient resolution to confirm the presence of this feature although it has already been noted by Schurr et al. (2006) that there are low velocities related to this volcano. The high velocity units are dominating the deeper portions where it is possible to observe the subducting slab in the depth slices at 150 and 200 km (Fig. 12C and D). The slices at 300 and 350 km depth show a group of low velocity asthenospheric anomalies between 70°W and 66°S (Fig. 12E and F) underlying the subducted slab that can be recognized to the east around 65°W. This is observed more clearly in the vertical

sections from Fig. 13A to C where the entire asthenosphere beneath the slab is associated with a low velocity body from 150 km downwards.

To analyze the distribution of velocity anomalies, we presented in Fig. 13, three west-east cross-sections at a spacing of 100 km. These profiles display the variation of the anomalies from north to south. The distribution and shape of the anomalies show that the low velocity zones can be separated into two groups in the north, form a single strong low-velocity region in the center and progressively become smaller and isolated to the south. We have created a conceptual cartoon to illustrate our interpretation of these anomalies.

### 3. Discussion

Here we present a tectonic and magmatic interpretation of a conception cartoon of the velocity anomalies shown on the three E–W and two N–S profiles in Fig. 17, which are inferred from the five tomographic cross-sections in Fig. 13. We then discuss how these features support a process of repeated and ongoing delamination (also called foundering) of the crustal and mantle lithosphere beneath the southern Puna plateau.

Starting with the northernmost W–E profile along line A, we point to the two striking low velocity anomalies (LV) on the opposite sides of the high velocity anomaly in the region of the Salar de Hombre Muerto block (HMB). These anomalies are in good agreement with

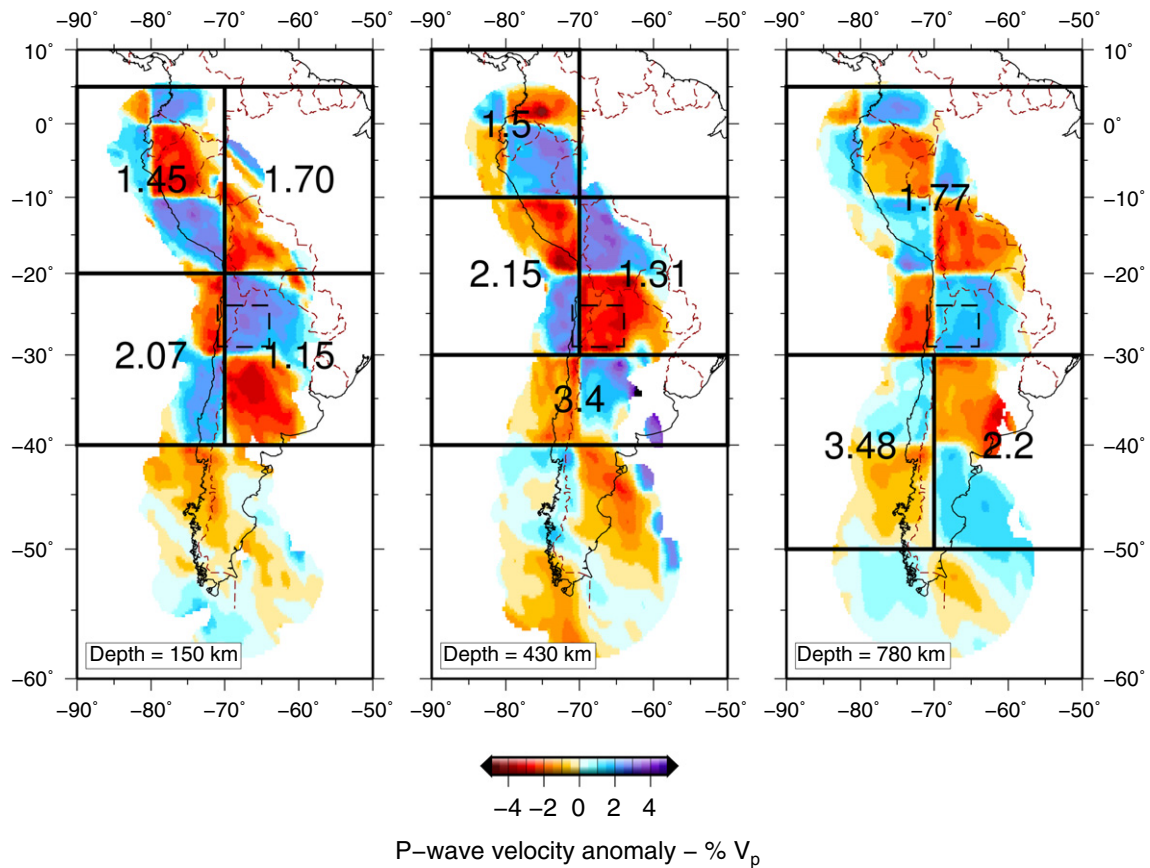


**Fig. 11.** Checkerboard resolution test of the global teleseismic inversion and the amplitude calibration values for different sub-regions used for correction of slab effect of the inversion of regional events. For each block in the checkerboard we computed the average recovered values. The inverted model will be multiplied by the calibration values for individual regions to warrant a full recovery of the original anomaly in the synthetic checkerboard model (i.e. 3%).

previous tomographic results in which branched low velocity zones to the west and east were interpreted as possible ascent paths for fluids and melts from the asthenosphere into the crust (e.g. Heit, 2005; Heit et al., 2008; Koulakov and Sobolev, 2006; Schurr et al., 2006). The western branch is indicated by the low velocity anomaly pointing towards the region of the Antofalla volcanic complex east of the volcanic arc, whereas the eastern branch is the one pointing towards the eastern side of the array in the Eastern Cordillera. The western low velocity anomaly is also clearly seen in the horizontal section at 35 km depth in Fig. 16, at which depth it likely coincides with the presence of partial melt in the crust. We call this low velocity anomaly, the Southern Puna Magmatic Body (SPMB). This anomaly coincides with a region of 6.7 Ma to Holocene mafic volcanism on the surface. It is also significant that there is no low velocity anomaly under the frontal CVZ arc region to the west where the volcanoes are currently considered to be inactive according to the Smithsonian catalog of active volcanism. The eastern low velocity anomaly, much of which is in the lower crust and uppermost mantle could also reflect fluids and melts related to the influx of hot asthenosphere in contact with continental lithosphere above the subducting slab. The youngest known surface volcanism to the east is related to the early Pliocene (~4.7 Ma) Antilla magmatic complex near 64.7°W (e.g. Gioncada et al., 2010).

Between these two low-velocity zones and beneath the Salar de Hombre Muerto just north of Cerro Galan, we designate the high velocity zone as the Hombre Muerto block (HMB). This block could be related to the high velocity region in the eastern border of the Puna plateau described by Heit (2005) as it coincides with the easternmost border of the plateau where Paleozoic granitic and metamorphic

rocks outcrop (e.g., Rapela et al., 1992). Another significant feature in the region of the Hombre Muerto block is that this is the area where Moho phases detected by P and S receiver functions suggest an anomalously thickened crust (ca. 80 km) relative to the surrounding region (Heit et al., 2010; Fig. 5). Below this high velocity block is another area of incipient high velocity between the base of the lithosphere and the slab at a depth near 100 km that is labeled DB?. This high velocity block could represent the remnants of a previously delaminated, foundered block.

Further south in Fig. 17B where the cross-section runs along the highest station density of the array, many of the same features occur. In comparison, the low velocity anomaly called the Southern Puna Magma Body is clearer than in Fig. 17A as the low velocities are concentrated in the center of the profile where they appear to be aligned beneath the near arc andesitic Cerro Peinado volcano and the backarc Cerro Blanco rhyolitic ignimbritic caldera. A number of other young mafic volcanoes between profiles A and B (e.g. Antofagasta, Jote, Alumbra volcanoes; see map in Risse et al., 2008) are also likely linked to this low velocity body, which extends as far east as 67°W. The distribution of these centers is consistent with profile B being in a region where the crust contains more partial melt than in profile A. The crustal low velocity anomalies appear to be related to partial melts trapped in the crust that were triggered by asthenospheric melts at depth (Kay et al., 2011a; Risse et al., to be submitted). As in profile A, the frontal volcanic arc to the west is disconnected from this area of low velocity consistent with the absence of currently active centers in this part of the CVZ arc.

The low velocity area in profile B just west of ~66°W extends towards the easternmost part of the array in the area of the Sierras

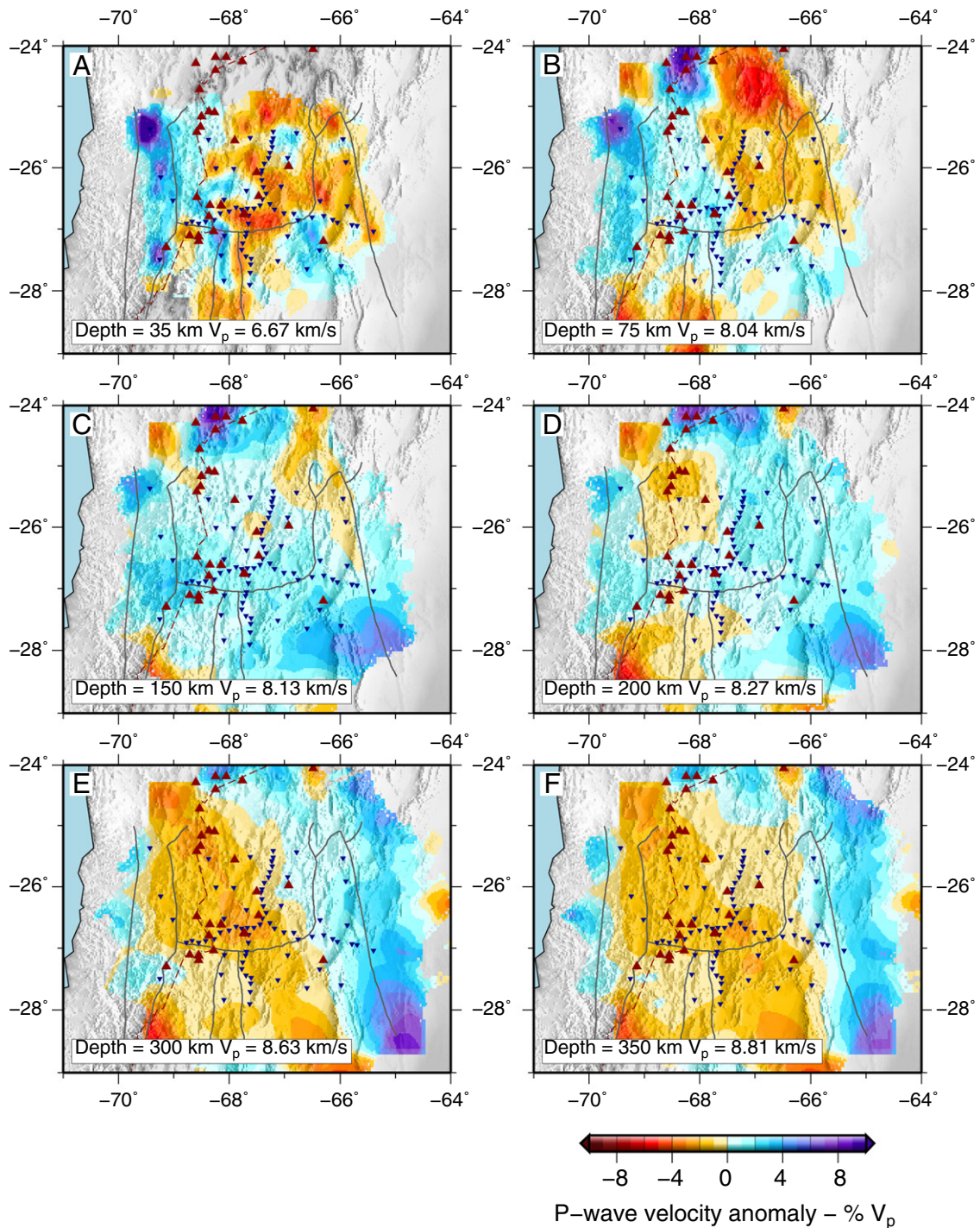


**Fig. 12.** Horizontal sections for the joint teleseismic-regional inversion (path (c) in Fig. 6). The inversion uses the model presented in Fig. 10 as a constraint. Red triangles are volcanoes. Stations are denoted by blue inverted triangles. Solid lines define the major tectonic units.

Pampeanas (Fig. 1A and B) where the most recent volcanism recorded on the surface is the earliest Pliocene volcanism at Farallon Negro (e.g. Sasso and Clark, 1998). The high velocity block in the crust at the border of the Puna plateau is clearly observed to be in the mid to lower crust in profile B with a part of it being beneath the crust. This block coincides with the region of Precambrian cratonic rocks from the Pampia Craton (e.g. Ramos et al., 1986). The Sierras Pampeanas block (SPB) could have played a key role in the evolution of the Puna Plateau to the south as it marks an abrupt end to the distribution of velocities in the Sierras Pampeanas–Puna Plateau border

region. The low velocity zone east of the SPB, in the crust and upper mantle could be linked to the area of transition between the Sierras Pampeanas, the Puna Plateau and the Santa Barbara System on the easternmost part of our array.

In the southernmost part of the array (Fig. 17C), a clear low velocity anomaly in the crust is concentrated in the volcanic arc where the large and potentially active Ojos del Salado and Tres Cruces volcanic centers are located (see summary in Kay and Mpodozis, 2002). Further east, a small low velocity region under the backarc is emplaced south of the main low velocity zone labeled SPMB in profile B whose

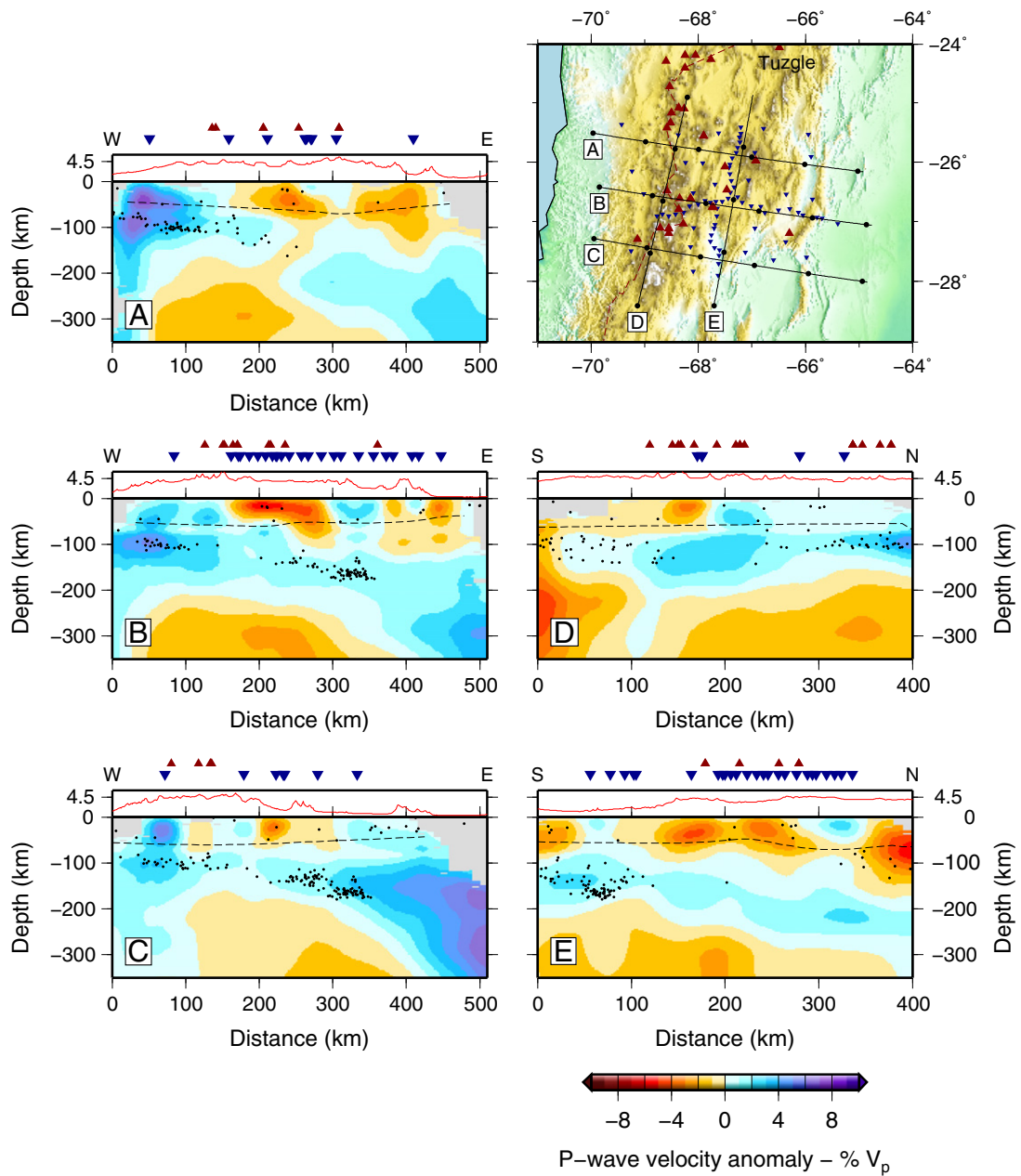


**Fig. 13.** Five cross sections from the inversion presented in Fig. 12. A, B and C are West–East profiles while D and E are South–North profiles. Inverted triangles are stations and red triangles are volcanoes. Tuzgle volcano is marked as reference for northern anomalies. The circles along the profile lines on the map are spaced every 100 km. Red lines on top of the profiles represent the topography and the black dots on the profiles are earthquakes extracted from a distance up to 150 km away from the profiles. Dashed lines in each section indicates the Moho depth from Fig. 5.

full extent is shown in the outlined region. This block is located beneath the Fiambola basin, which is part of the Famatina System region between the main Andean Cordillera Frontal and the Pampean ranges, in an area of hot springs and hydrothermal activity. The low velocity region on the eastern border of the array as seen in profiles A and B is not present in profile C where its place is occupied by the high velocity SPB consistent with the asthenosphere in this region being cooler than to the north and with the lack of backarc volcanism. The decrease in the dip of the subducting Nazca plate under his region is also clearly seen in the high velocity anomaly near 100 km depth.

The south–north profile along the volcanic arc shown in Fig. 17D reveals a low velocity body beneath the Ojos del Salado volcano and a high velocity block to the north, which is probably related to the

effects of the subducting slab. Kay et al. (2011b) suggested the high velocity region might reflect forearc lithosphere built up as a result of subduction erosion associated with frontal arc migration (Goss and Kay, 2009; Kay and Mpodozis, 2002). As in profiles A and B, there is no low velocity anomaly associated with the currently inactive CVZ frontal arc centers north of the Ojos del Salado volcano. Another outstanding feature in this section is the north–south trending slab that remains at a constant depth of ~100 km. The changes in the dip of the subduction from north to south has not yet began at this depth, as well indicated by the slab contours in Fig. 1A.

The profile in Fig. 17E runs parallel to the highest south–north station density of our seismic array. A low velocity area in the south of this profile is outside of the array and the area of lines of confidence of

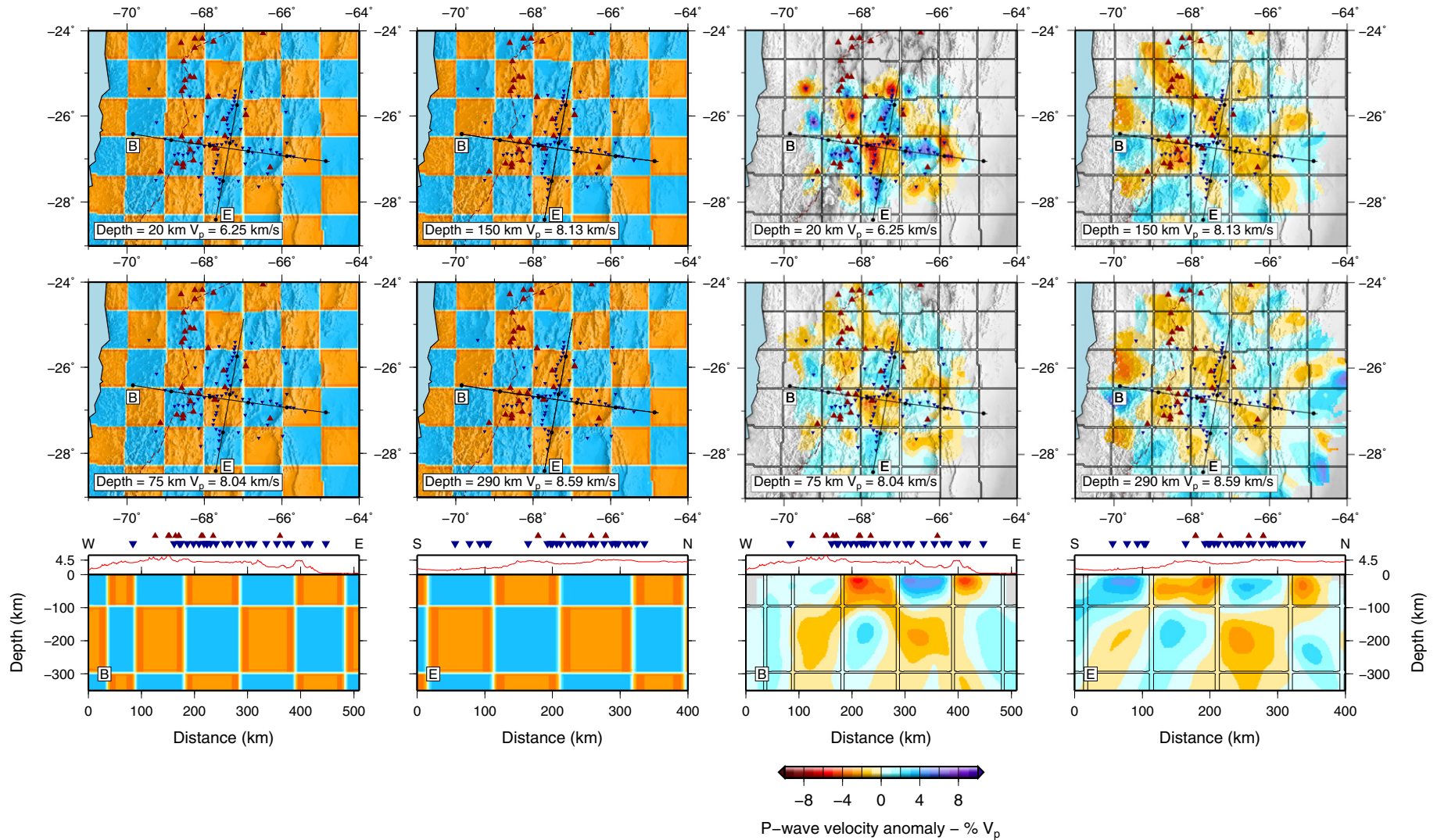


**Fig. 14.** Checkerboard test for the inversion path (c) shown in Fig. 6. For performing this test we used the events and stations locations as in the real scenario. The first and second columns represent the synthetic model ( $100 \times 100$  km checkerboard) for horizontal and vertical sections. The results of the test are presented in columns 3 and 4. Stations are the inverted blue triangles, volcanoes are the red triangles. In columns 3 and 4 the squares are the contours of the synthetic models as presented in column 1 and 2. The vertical sections tests are performed following the position of the vertical profiles (black lines B and E).

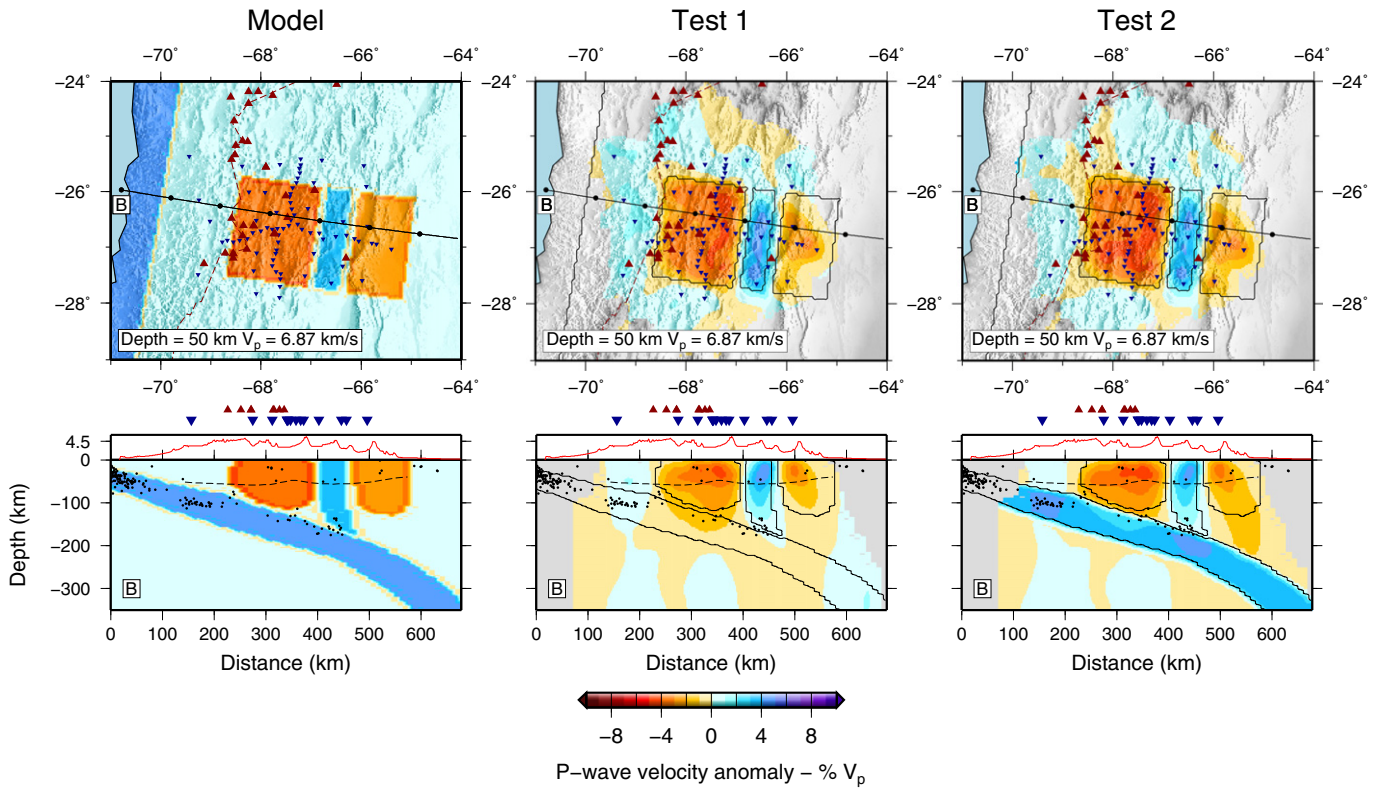


**Fig. 15.** Synthetic test performed using the slab a-priori information. In the left column (Model) we present the synthetic model used for the forward modeling. The middle column (Test 1) is the result of the inversion without a-priori information of the slab. The right column (Test 2) is the result when the slab a-priori information is used in the inversion as done in the inversion path (c) from Fig. 6. The correct slab a-priori information does not affect the results for the crust and upper mantle. It can help to trace the rays more accurately for the regional events and to avoid projecting the slab high velocity anomaly outside the study area into the model.

our data. In the center of the profile, we see the large low velocity anomaly labeled SPMB in profiles A and B. In the north–south profile D, it is possible to see that this low velocity anomaly extends from

north of the intersection with profile C to the southern edge of the Hombre Muerto high velocity block (HMB). North of the Hombre Muerto block, another low velocity body overlaps the lower crust and uppermost mantle. This anomaly extends northward towards the young Tuzgle volcano (Coira and Kay, 1993), which is outside our array but that has been shown to be associated with a strong low velocity anomaly attributed to delamination by Schurr et al. (2003). In this region, many young volcanic centers are associated with high electrical conductive anomalies detected by magnetotellurics (e.g. Díaz et al., 2012; Lezaeta and Brasse, 2001).

Profile E also shows the same high velocity anomalies in the crust and mantle shown in profile A. They are recognizable as the anomaly labeled the Hombre Muerto Block (HMB) in the crust and the weaker anomaly labeled DB? for delaminated or foundered lithospheric block. The southward shallowing of the subducting Nazca plate is also well illustrated by the high velocity anomaly corresponding to the slab that runs from ~200 km depth in the north to near 100 km depth in the south.

The region to the south of the study area is marked by the volcanic gap related to the low subduction angle of the Nazca plate (Fig. 10, Section 4), which is alternatively known as the Chilean, Pampean or Chilean–Pampean flat-slab (e.g. Cahill and Isacks, 1992). The causes for the flat-slab segment remain controversial, but many authors have suggested its origin is related to the subduction of the Juan Fernandez Ridge (e.g., Kay and Mpodozis, 2002; Yáñez et al., 2001). Recently, Gans et al. (2011) improved the quality of the Moho topography over the flat-slab by using receiver functions and suggested that the flattening is consistent with being the result of the subduction of over-thickened oceanic crust along the trace of the Juan Fernandez Ridge. A number of other authors based on results from seismic studies in the flat-slab region south of our array have shown the topography of

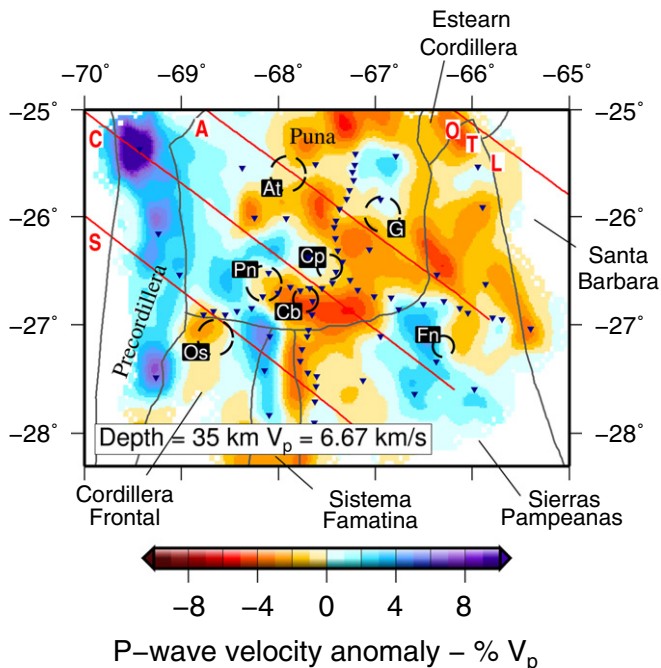


**Fig. 16.** Horizontal tomographic section at a depth of 35 km together with the geological features and volcanoes. Abbreviations and symbols are the same as in Fig. 1.

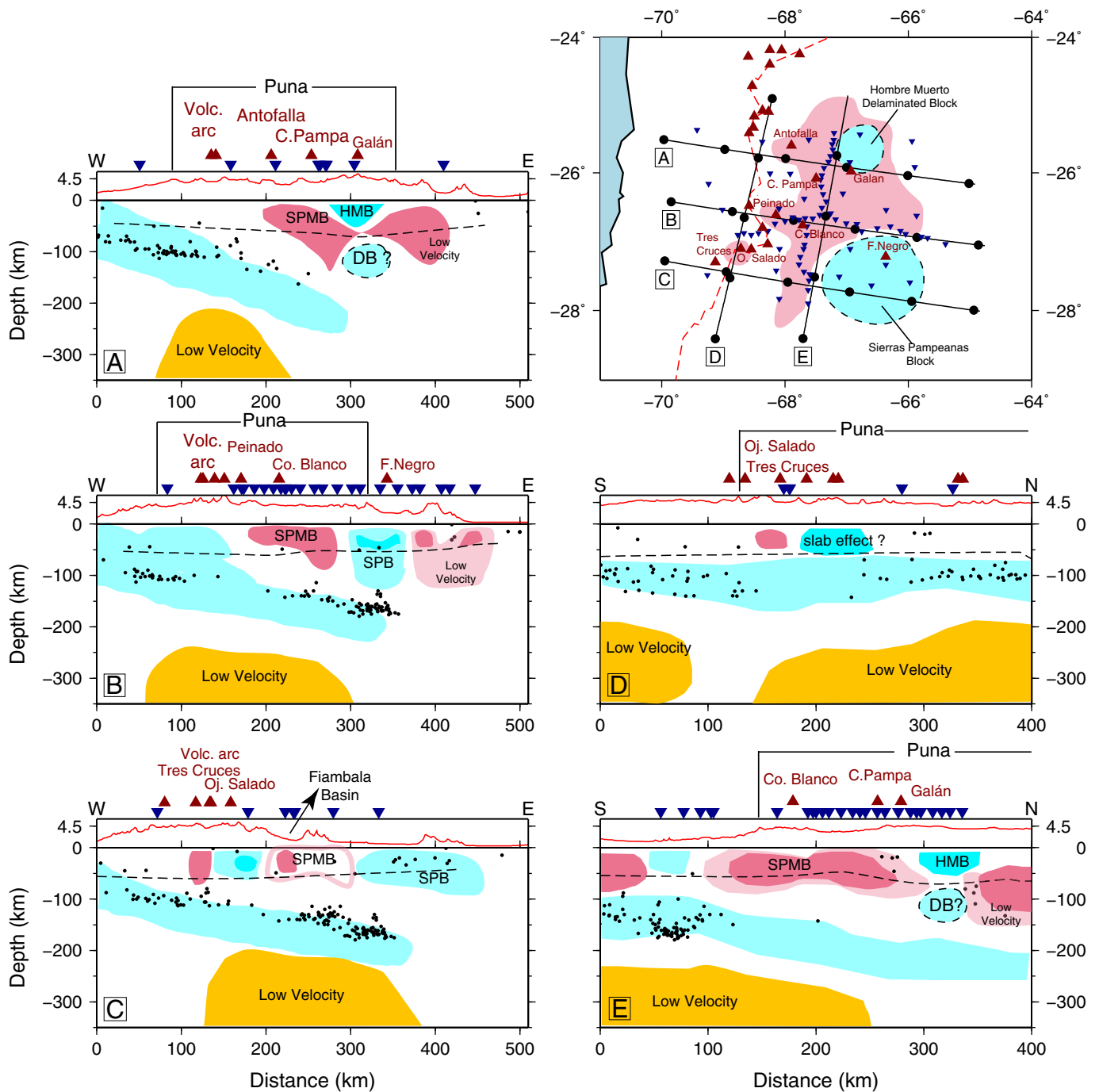


**Fig. 17.** Interpretation cartoon of the results presented in Fig. 13. Low velocities are denoted in orange in the mantle beneath the slab and in red and pink in the lithosphere and asthenosphere above the slab, respectively. High velocities are in light blue. Abbreviations: SPMB – Southern Puna Magmatic Body; HMB – Hombre Muerto Block; DB ? – Delaminated Block; SPB – Sierras Pampeanas Block. On the map (top right) the different profiles are shown along with the position at the surface marked as reference of two high velocity blocks (DB and SPB) and the low-velocity areas described in the text.

the continental Moho (e.g. Alvarado et al., 2005, 2007; Fromm et al., 2004; Gilbert et al., 2006; Heit et al., 2008). As in the sections of our tomographic images south of 27.5°S (Fig. 10, Section 4; Fig. 13 profiles C, D, and E), reliable low velocity anomalies are sparsely distributed in the crust. The low velocity anomalies appearing on our profile C are near 69°W where the active CVZ volcanic arc begins. The contrast with our profiles to the north is consistent with a distinctively cooler thermal regime in the flat-slab region than in the Puna where lithospheric low velocity anomalies are widespread. As pointed out by Barazangi and Isacks (1976), the flattening of the subducting slab

results in a reduction in the asthenospheric wedge leading to a restricted evolution and movement of fluids and magma in the narrowed mantle wedge.

The tomographic sections in Fig. 13 also show large low velocity anomalies of various dimensions below the slab. These low velocity anomalies are distributed across the area but tend to be concentrated just behind the volcanic front and where the slab tends to be shallower and flatter in the backarc. These low velocities (Fig. 17A to E) might be related to a hot asthenospheric mantle as discussed by Woelber et al. (2009).



#### 4. Relationship to the delamination model

A number of features in the tomographic images of the southern Puna could be consistent with the delamination model proposed by Kay et al. (1994) in the region of the Cerro Galan caldera and amplified into a model for repeated delamination over a steepening subduction zone since the latest Miocene by Kay and Coira (2009). Evidence for delamination was based on the late Miocene to Quaternary eruptions of the Cerro Galan ignimbritic center, a concentration of <7 Ma primitive mafic lavas in the southern Puna generally associated with faults that formed in response to change in the regional stress regime, high pressure chemical signatures in evolved magmas, a high average regional elevation and seismic evidence for a thin underlying lithosphere and an abnormally hot subducting slab.

In addressing the evidence for previous delamination, we point to the high velocity region in the asthenosphere that we interpret as the remnants of a delaminated lithospheric block (DB?) that could be linked to the formation of the ~2 Ma Galan ignimbrite. Supporting evidence for delamination also comes from the distribution of low velocity zones. In particular, we consider the position of the high velocity DB block surrounded by low velocity anomalies to the south, north and west to be significant as we attribute these low velocity anomalies to regions of thinned lithospheric mantle where decompression mantle melts have triggered partial melting in the crust. It is particularly significant that the low velocity anomaly to the south and west, which corresponds to the Southern Puna Magma body (SPMB), is associated with repeated mafic surface volcanism that began at ~6.7 Ma. The removal of the delaminated lithosphere would allow the influx of asthenospheric material seen on west–east profile that crosses the Cerro Galan region on Fig. 17A. The low velocity anomaly in the north seen on the south–north profile 17 E is also over a region of repeated mafic volcanism. Thus, both the mafic volcanism and the Cerro Galan ignimbrites are consistent with a link to foundering and delamination of the underlying lithosphere. The key to this argument is if the material from the delaminated Puna lithosphere is really what is seen in the high velocity region interpreted as the delaminated block. If this feature is not well resolved, further tomographic studies using local earthquakes could help us to shed light on this question. The other lingering question is the origin of the low velocity anomalies in the east on profiles 17A and 17B, where the youngest volcanism at the surface is early Pliocene in age.

The question as to why delamination events would be triggered north of the Cerro Galan region could be related to the presence of a pre-existing dense crust under this area, which was residual to the prominent Ordovician arc (e.g., Rapela et al., 1992; Coira et al., 1999) that existed in this area. The region is also unique in being near the important structural transition east of the Puna at 26°S which separates the Eastern Cordillera and the Santa Barbara belt to the north from the Sierras Pampeanas to the south (Fig. 1). In addition, Andean contractional deformation would lead to further crustal thickening enhancing the instability of a thick crust with an eclogitic base that in turn could trigger lithospheric delamination (or foundering).

The major eruptions of the Cerro Galan caldera also largely coincide with the principal pulses in the post 8–7 Ma uplift of the Sierras Pampeanas to the east, suggesting a possible cause and effect relationship (see Kay and Coira, 2009; Kay et al., 2011a). One possible model is that contraction-related failure of the melt weakened crust beneath Cerro Galan squeezed out partial melts from the mid to deep crust to produce the ephemeral magma chambers that erupted the ignimbrites, including the giant Galan ignimbrite (500 km<sup>3</sup>) at ~2 Ma. Renewed thickening of the crust in these periods could also partially explain the thick crust inferred from the receiver function analyses. The high velocity tomographic anomaly in profile A could

thus be partly related to granulitic and eclogitic crust created in the course of crustal thickening as mantle-derived basaltic melts produced the hybrid melts that later became the ignimbrites. A complementary explanation for the high velocity Hombro Muerto crustal block is that this region coincides with an area of incomplete crustal delamination in previous events. A dense residual thickened crust sets the scene for a future episode of lower crustal and lithospheric foundering or delamination in a repeated cycle. Temporal variations in mantle-derived mafic magma chemistry fit with Neogene mantle enrichment by introduction of crustal material into the mantle during the subduction and delamination process (e.g. Kay and Mpodozis, 2001, 2002).

In this vein, the tomographic images presented here might suggest that the delamination process in this region is still on-going. In particular, the images show the Hombro Muerto high velocity body block (HMB) in the crust on the northern margin of the Cerro Galan region, which is also apparently a concentrated region of very thick crust (Fig. 5). We speculate that this high velocity anomaly is thickened, dense crust that could be a trigger for a future period of delamination. A high lithostatic pressure could assist in the eclogite phase transition and help to stimulate the delamination process.

#### 5. Conclusions

Seismic images of the Southern Puna crust and upper mantle are largely dominated by the subducting Nazca slab and the low velocities related to the volcanism possibly originating from lithospheric delamination in the north of our study area. Benefiting from the joint inversion of regional, teleseismic and the global ISC catalog data, the subducted oceanic lithosphere of the Nazca plate has been clearly observed. Being in a transition zone from normal to flat subduction, the slab shallows from north to south by ~100 km. The main velocity anomalies across the region are emplaced in areas with crustal thicknesses ranging from about 50 to 80 km. The anomalies are also related to a mid-crustal back arc melt zone under the southern Puna, and might represent evidence for delaminating or recently delaminated lithospheric blocks. The velocities are low where the crust is thin in the center of the plateau and high in the area where the crust is thick in the Galan area.

The tomographic images suggest that the thermal state of the Puna plateau is relatively hot as suggested by Whitman et al. (1992, 1996) and Heit et al. (2008). This thermal effect can be interpreted on the basis of the extension of the crustal low velocity body that we call here the Southern Puna Magmatic Body (SPMB). The SPMB stretches from the south towards the north of the array in connection with most of the prominent volcanic fields in the back arc.

The Southern Puna Magma Body could be disconnected from the Altiplano Puna Low Velocity body described for the northern Puna and the Altiplano plateaus by Yuan et al. (2000). The limit between the SPMB and the Altiplano Puna Low Velocity (APLV) zone could be related to the presence of the Olacapato-Toro lineament in the north of the array which is responsible for the differences between the southern and northern Puna areas.

Only the Archibarca lineament seems to correlate well with our results while the others lineaments to the south do not seem to be inducing any changes in the distribution of velocities in the crust. Although some local velocity variations can be seen along the trace of these crustal lineaments (e.g. Peinado and C. Blanco volcanoes with lineament C), most of the velocity variations are not observed along the entire extension of the lineaments and might therefore be controlled only locally.

The volcanic arc seems to be disconnected from the SPMB and only correlates with low velocities in the area of the Ojos del Salado-Tres Cruces volcanic field in the southwest of the array. The Culampaja and Ojos del Salado lineaments could play a key role in

the distribution of the anomalies. As in the case of the Archibarca lineament, attributed to an area where the Antofalla volcanic complex and the Cerro Galan caldera are located, these crustal lineaments might be regulating the movement of fluids within the crust. This is best observed in Fig. 16 where there appears to be a correlation between the different lineaments in the Puna and the position and distribution of low velocities in the crust at a depth of 35 km.

The late Miocene centers further east (i.e. Farallon Negro) represent the easternmost volcanic centers in the southern Puna and indicate that the region has been subject to volcanic activity at different stages in the geodynamic evolution of the plateau. This volcanic activity seems to correlate well with the distribution of anomalies in the center of the array where it is possible to delineate most of them with the presence of intra-crustal magma chambers in the plateau. Probably, these older volcanic centers are reflecting the story of the shallowing and steepening of the subduction zone as suggested by Kay and Coira (2009). The abrupt change in velocities at the southernmost end of the Puna Plateau coincides with the region of crystalline basement rocks from the Pampia Craton which could have imposed a barrier for the Puna growth to the south. The Pampean lithosphere could be therefore responsible for the evolution of the plateau and the distribution of deformation and volcanism in this region.

As discussed above, the ~6.7 to 2 Ma activity of the Cerro Galan ignimbrite caldera complex has been postulated to be related to crustal and mantle lithospheric delamination that lead to decompression melting that produced the mantle basaltic melts that triggered crustal melting that produced the ignimbrites (e.g., Kay et al., 1994, 1999, 2011a). Contemporaneous mafic lavas erupted from the Salar de Hombre Muerto in the north to the Cerro Blanco region in the south during this same time are also suggested to be triggered by this delamination event. This delamination model is supported by our tomographic images where we see a good correlation between the distribution of low velocity anomalies in the mantle and crust and the position of these mafic volcanic centers and a high velocity region in the mantle that could represent the delaminated block in the north of our study area.

Finally, the distribution of velocities north and south of the Hombre Muerto Block and the incipient evidence for delaminated material in the upper mantle could be indicating that beneath Galan the delamination process already happened. The process could be still active induced by the thicker crust currently under the effects of higher lithostatic pressures that could stimulate the delamination process and thus could continue delaminating to the north in the future.

## Acknowledgements

We would like to thank the German Research Centre for Geosciences GFZ and the German Research Council (DFG) for the funding. The equipment has been provided by Geophysical Instrument Pool Potsdam (GIPP). Similarly this project would not have been possible without funding from the National Science Foundation EAR Grant (0538112) Foundation Grant and IRIS PASSCAL. Continuous waveform data are archived at the IRIS and GEOFON data centers. We thank Marcelo Assumpcao and an anonymous reviewer for comments and suggestions that helped us to improve the MS. We also thank Bob Kay for comments and discussion on the results. The array benefited from land owners and farmers in Catamarca, Salta and Tucuman who kindly provided a secure place for the stations during two years.

## References

- Allmendinger, R.W., Jordan, T.E., Kay, S.M., Isacks, B., 1997. The evolution of the Altiplano-Puna Plateau of the Central Andes. *Annual Review of Earth and Planetary Sciences* 25, 139–174.
- Alonso, R.N., Viramonte, J.G., Gutierrez, R., 1984. Puna Austral. Bases para el subprovincialismo geológico de la Puna Argentina. IX Congreso Geológico Argentino, Bariloche, Actas I, pp. 43–63.
- Alvarado, P., Beck, S., Zandt, G., Araujo, M., Triep, E., 2005. Crustal deformation in the south-central Andes backarc terranes as viewed from regional broad-band seismic waveform modelling. *Geophysical Journal International* 163, 580–598. <http://dx.doi.org/10.1111/j.1365-246X.2005.02759.x>.
- Alvarado, P., Beck, S., Zandt, G., 2007. Crustal structure of the south-central Andes Cordillera and backarc region from regional waveform modelling. *Geophysical Journal International* 170, 858–875. <http://dx.doi.org/10.1111/j.1365-246X.2007.03452.x>.
- Barazangi, M., Isacks, B., 1976. Spatial distribution of earthquakes and subduction of the Nazca plate beneath South America. *Geology* 4, 686–692.
- Cahill, T., Isacks, B.L., 1992. Seismicity and shape of the subducted Nazca plate. *Journal Of Geophysical Research-Solid Earth* 97, 17503–17529.
- Coira, B., Kay, S.M., 1993. Implications of Quaternary volcanism at Cerro Tuzgle for crustal and mantle evolution of the Puna Plateau, Central Andes, Argentina. *Contributions to Mineralogy and Petrology* 113, 40–58. <http://dx.doi.org/10.1007/BF00320830>.
- Coira, B., Pezzutti, N., 1976. Vulcanismo cenozoico en el ámbito de La Puna catamarqueña (25°30'–25°50' Lat. S y 68°–68°30' Long. O.). *Asociación Geológica Argentina Revista* 31, 33–52.
- Coira, B., Kay, S.M., Viramonte, J., 1993. Upper Cenozoic magmatic evolution of the Argentine Puna – a model for changing subduction geometry. *International Geology Review* 35, 677–720.
- Coira, B., Kay, S.M., Pérez, B., Woll, B., Hanning, M., Flores, P., 1999. Magmatic sources and tectonic setting of Gondwana margin Ordovician magmas, Northern Puna of Argentina and Chile. In: Ramos, V.A., Keppie, D. (Eds.), *Laurentian-Gondwana Connections Before Pangea: Geological Society of America Special Paper*, 336, pp. 145–170.
- de Silva, S., Gosnold, 2007. Episodic construction of batholiths: insights from the spatiotemporal development of an ignimbrite flare-up. *Journal of Volcanology and Geothermal Research* 167, 320–325.
- Díaz, D., Brasse, H., Ticona, F., 2012. Conductivity distribution beneath Lascar volcano (Northern Chile) and the Puna, inferred from magnetotelluric data. *Journal of Volcanology and Geothermal Research* 217–218, 21–29. <http://dx.doi.org/10.1016/j.jvolgeores.2011.12.007> (ISSN 0377-0273).
- Evans, J., Achauer, U., 1993. Teleseismic velocity tomography using the ACH method: theory and application to continental scale studies. In: Iyer, H., Hirahara, K. (Eds.), *Seismic Tomography: Theory and Practice*. Chapman and Hall, London, pp. 319–360.
- Francis, P.W., Sparks, R.S.J., Hawkesworth, C.J., Thorpe, R.S., Pyle, D.M., Tait, S.R., Mantovani, M.S.M., McDermott, F., 1989. Petrology and geochemistry of volcanic rocks of the Cerro Galan caldera, northwest Argentina. *Geological Magazine* 126, 515–547.
- Fromm, R., Zandt, G., Beck, S.L., 2004. Crustal thickness beneath the Andes and Sierras Pampeanas at 30°S inferred from Pn apparent phase velocities. *Geophysical Research Letters* 31. <http://dx.doi.org/10.1029/2003GL019231>.
- Gans, C.R., Beck, S.L., Zandt, G., Gilbert, H., Alvarado, P., Anderson, M., Linkimer, L., 2011. Continental and oceanic crustal structure of the Pampean flat slab region, western Argentina, using receiver function analysis: new high-resolution results. *Geophysical Journal International* 186, 45–58. <http://dx.doi.org/10.1111/j.1365-246X.2011.05023.x>.
- Gilbert, H., Beck, S., Zandt, G., 2006. Lithospheric and upper mantle structure of central Chile and Argentina. *Geophysical Journal International* 165, 383–398.
- Gioncada, A., Vezzoli, L., Mazzuoli, R., Omarini, R., Nonnotte, P., Guillou, H., 2010. Pliocene intraplate-type volcanism in the Andean Foreland at 26 degrees 10'S, 64 degrees 40'W (NW Argentina): implications for magmatic and structural evolution of the Central Andes. *Lithosphere* 2 (3), 153–171. <http://dx.doi.org/10.1130/L81.1>.
- Goss, A.R., Kay, S.M., 2009. Extreme high field strength element (HFSE) depletion and near-chondritic Nb/Ta ratios in Central Andean adakite-like lavas (27° S, 68° W). *Earth and Planetary Science Letters* 270, 97–109.
- Heit, B., 2005. Teleseismic tomographic images of the Central Andes at 21°S and 25.5°S: an inside look at the Altiplano and Puna plateaus, Ph.D Thesis, Freie Universitaet Berlin, Scientific Technical Report (STR06/05), Geoforschungszentrum, Potsdam- Germany.
- Heit, B., Sodoudi, F., Yuan, X., Bianchi, M., Kind, R., 2007. An S-receiver function analysis of the lithospheric structure in South America. *Geophysical Research Letters* 34, L14307. <http://dx.doi.org/10.1029/2007GL030317>.
- Heit, B., Koulakov, I., Asch, G., Yuan, X., Kind, R., Alcozer, I., Tawakkoli, S., Wilke, H., 2008. More constraints to determine the seismic structure beneath the Central Andes at 21°S using teleseismic tomography analysis. *Journal of South American Earth Sciences* 25, 22–36.
- Heit, B., Yuan, X., Kumar, P., Kind, R., Kay, S.M., Sandvol, E.A., Alonso, R., Coira, B., Comte, D., Brown, L.D., 2010. Crustal investigations in the southern Puna plateau by receiver functions from the Puna Delamination (PUDEL project) seismic array in the Central Andes. Abstract T13D-05 presented at 2010 Fall Meeting, AGU, San Francisco, Calif., 13–17 Dec.
- Isacks, B., 1988. Uplift of the central Andean plateau and bending of the Bolivian orocline. *Journal of Geophysical Research* 93 (B4). <http://dx.doi.org/10.1029/88JB01309>. issn: 0148-0227.
- Kay, S.M., Coira, B., 2009. Shallowing and steepening subduction zones, continental lithosphere loss, magmatism and crustal flow under the Central Andean Altiplano-Puna Plateau. In: Kay, S.M., Ramos, V.A., Dickinson, W.M. (Eds.), *Backbone of the Americas: Shallow Subduction, Plateau and Ridge and Terrane Collisions: Geological Society of America Memoir*, 204, pp. 229–260.
- Kay, R., Kay, S.M., 1993. Delamination and delamination magmatism. *Tectonophysics* 219, 177–189.
- Kay, S.M., Mpodozis, C., 2001. Central Andean ore deposits linked to evolving shallow subduction systems and thickening crust. *GSA Today* 11 (3), 4–9.

- Kay, S.M., Mpodozis, C., 2002. Magmatism as a probe to the Neogene shallowing of the Nazca Plate beneath the modern Chilean flat-slab. *Journal of South American Earth Sciences* 15, 39–57.
- Kay, S.M., Coira, B., Viramonte, J., 1994. Young mafic back arc volcanic rocks as indicator of continental lithospheric delamination beneath the Argentine Puna plateau, central Andes. *Journal of Geophysical Research* 99, 24323–24339.
- Kay, S.M., Mpodozis, C., Coira, B., 1999. Neogene magmatism, tectonism, and mineral deposits of the Central Andes (22° to 33° latitude). In: Skinner, B.J. (Ed.), *Geology and Ore Deposits of the Central Andes: Society of Economic Geology Special Publication*, 7, pp. 27–59.
- Kay, S.M., Coira, B.L., Caffè, P.J., Chen, C.-H., 2010. Regional chemical diversity, crustal and mantle sources and evolution of the Neogene Puna plateau ignimbrites of the Central Andes. *Journal of Volcanology and Geothermal Research* 198, 81–111.
- Kay, S.M., Coira, B., Wörner, G., Kay, R.W., Singer, B.S., 2011a. Geochemical, isotopic and single crystal <sup>40</sup>Ar/<sup>39</sup>Ar age constraints on the evolution of the Cerro Galán ignimbrites. *Bulletin of Volcanology* 73, 1487–1511.
- Kay, S.M., Liang, X., Sandvol, E.A., Heit, B., Mulcahy, P., Chen, C., Yuan, X., Coira, B.L., Brown, L.D., 2011b. Seismic and magmatic evidence for continental lithospheric evolution on the Andean Margin beneath the Central Volcanic Zone (CVZ) Arc and Southern Puna Plateau (25°S–28°S) since 8 Ma. Abstract T131-05, Fall Meeting, AGU, San Francisco.
- Kley, J., Monaldi, C., 1998. Tectonic shortening and crustal thickness in the Central Andes: how good is correlation? *Geology* 26, 723–726.
- Kley, J., Monaldi, C.R., Salfity, J.A., 1999. Along-strike segmentation of the Andean foreland: causes and consequences. *Tectonophysics* 301, 75–94.
- Koulakov, I., 2009. LOTOS code for local earthquake tomographic inversion: benchmarks for testing tomographic algorithms. *Bulletin of the Seismological Society of America* 99, 194–214.
- Koulakov, I., Sobolev, S.V., 2006. Moho depth and three-dimensional P and S structure of the crust and uppermost mantle in the Eastern Mediterranean and Middle East derived from tomographic inversion of local ISC data. *Geophysical Journal International* 164 (1), 218–235.
- Lezaeta, P., Brasse, H., 2001. Electrical conductivity beneath the volcanoes of the NW Argentinian Puna. *Geophysical Research Letters* 28, 4651–4654.
- Marrett, R.A., Allmendinger, R.W., Alonso, R.N., Drake, R.E., 1994. Late Cenozoic tectonic evolution of the Puna plateau and adjacent foreland, northwestern Argentine Andes. *Journal of South American Earth Sciences* 7, 179–207.
- McGlashan, N., Brown, L.D., Kay, S.M., 2008. Crustal thicknesses in the Central Andes from teleseismically recorded depth phase precursors. *Geophysical Journal International* 175, 1013–1022.
- Mulcahy, P., 2012. The southern Puna seismic experiment: seismicity and the morphology of the subduction zone. M.S. thesis, Cornell University, 84 pp.
- Mulcahy, P., Chen, C., Kay, S.M., Brown, L.D., Alvarado, P.M., Sandvol, E.A., Heit, B., Yuan, X., 2010. The Southern Puna seismic experiment: shape of the subducting Nazca Plate, areas of concentrated mantle and crustal earthquakes, and crustal focal mechanisms. Fall Meet. Suppl., *Eos Trans. AGU*, 91(53) (Fall Meet. Suppl., Abstract T11A-2050).
- Oncken, O., Hindle, D., Kley, J., Elger, K., Victor, P., Schemmann, K., 2006. Deformation of the Central Andean upper plate system—facts, fiction, and constraints for plateau models. In: Oncken, O., et al. (Eds.), *The Andes—Active Subduction Orogeny*. *Frontiers in Earth Sciences*, 1. Springer-Verlag, Berlin, pp. 3–28.
- Prezzi, C., Götze, H.-J., Schmidt, S., 2009. 3D density model of the Central Andes. *Physics of the Earth and Planetary Interiors* 177 (3–4), 217–234. <http://dx.doi.org/10.1016/j.pepi.2009.09.004> (ISSN 0031-9201).
- Ramos, V.A., 1999. Las provincias geológicas del territorio argentino. *Geología Argentina*. In: Caminos, R. (Ed.), *SEGEMAR. Anales*, 29 (3), pp. 41–96.
- Ramos, V.A., Jordan, T.E., Allmendinger, R.W., Mpodozis, C., Kay, S.M., Cortés, J.M., Palma, M., 1986. Paleozoic terranes of the central Argentine-Chilean Andes. *Tectonics* 5 (6), 855–880.
- Rapela, C.W., Coira, B., Toselli, A.J., Saavedra, J., 1992. El magmatismo del Paleozoico Inferior en el Sudoeste de Gondwana. In: Gutiérrez-Marco, et al. (Eds.), *El Paleozoico Inferior de Iberoamérica*, pp. 21–68.
- Richards, P.R., Ullrich, T., Kerrich, R., 2006. The late Miocene–Quaternary Antofalla volcanic complex, southern Puna, NW Argentina: protracted history, diverse petrology, and economic potential. *Journal of Volcanology and Geothermal Research* 152, 197–239.
- Riller, U., Oncken, O., 2003. Growth of the Central Andean Plateau by tectonic segmentation is controlled by the gradient in crustal shortening. *Journal of Geology* 111 (3), 367–384.
- Risse, A., Trumbull, R.B., Coira, B., Kay, S.M., van den Bogaard, P., 2008. <sup>40</sup>Ar/<sup>39</sup>Ar geochronology of basaltic volcanism in the back-arc region of the southern Puna plateau, Argentina. *Journal of South American Earth Sciences* 26, 1–15.
- Sasso, A.M., Clark, A.H., 1998. The Farallón Negro group, northwest Argentina: magmatic, hydrothermal and tectonic evolution and implications for Cu–Au metallogeny in the Andean back-arc. *Society of Economic Geologists Newsletter* 34 (1), 8–18.
- Schurr, B., Asch, G., Rietbrock, A., Kind, R., Pardo, M., Heit, B., Monfret, T., 1999. Seismicity and average velocities beneath the Argentine Puna plateau. *Geophysical Research Letters* 26, 3025–3028.
- Schurr, B., Asch, G., Rietbrock, A., Trumbull, R., Haberland, C., 2003. Complex patterns of fluid and melt transport in the central Andean subduction zone revealed by attenuation tomography. *Earth and Planetary Science Letters* 215, 105–119.
- Schurr, B., Rietbrock, A., Asch, G., Kind, R., Oncken, O., 2006. Evidence for lithospheric detachment in the central Andes from local earthquake tomography. *Tectonophysics* 415 (1–4), 203–223. <http://dx.doi.org/10.1016/j.tecto.2005.12.007>.
- Scire, A.C., Berk Biryol, C., Beck, S.L., Zandt, G., Gray, G., Heit, B., 2011. Data mining for teleseismic tomography in the central Andes. AGU 2011 Fall Meeting (San Francisco 2011).
- Sparks, R.S.J., Francis, P.W., Hamer, R.D., Pankhurst, R.J., O’Callaghan, L.O., Thorpe, R.S., Page, R., 1985. Ignimbrites of the Cerro Galán Caldera, NW Argentina. *Journal of Volcanology and Geothermal Research* 24, 205–248.
- Tassara, A., Götze, H.-J., Schmidt, S., Hackney, R., 2006. Three-dimensional density model of the Nazca plate and the Andean continental margin. *Journal of Geophysical Research* 111, B09404. <http://dx.doi.org/10.1029/2005JB003976>.
- Whitman, D., Isacks, B.L., Chatelain, J.-L., Chiu, J.-M., Perez, A., 1992. Attenuation of high-frequency seismic waves beneath the central andean plateau. *Journal of Geophysical Research* 97, 19929–19947.
- Whitman, D., Isacks, B., Kay, S.M., 1996. Lithospheric structure and along-strike segmentation of the Central Andean Plateau; seismic Q, magmatism, flexure, topography and tectonics. *Tectonophysics* 259 (1–3), 29–40.
- Woelbern, I., Heit, B., Yuan, X., Asch, G., Kind, R., Viramonte, J., Tawackoli, S., Wilke, H., 2009. Receiver function images from the Moho and the slab beneath the Altiplano and Puna plateaus in the Central Andes. *Geophysical Journal International* 177, 296–308.
- Yáñez, G., Ranero, C.R., von Huene, R., Díaz, J., 2001. Magnetic anomaly interpretation across the southern central Andes (32°–34°S): the role of the Juan Fernández Ridge in the late Tertiary evolution of the margin. *Journal of Geophysical Research* 106, 6325–6345.
- Yuan, X., Sobolev, S.V., Kind, R., Oncken, O., Bock, G., Asch, G., Schurr, B., Graeber, F., Rudloff, A., Hanka, W., Wylegalla, K., Tibi, R., Haberland, C., Rietbrock, A., Gliese, P., Wigger, P., Rower, P., Zandt, G., Beck, S., Wallace, T., Pardo, M., Comte, D., 2000. Subduction and collision processes in the Central Andes constrained by converted seismic phases. *Nature* 408, 958–961. <http://dx.doi.org/10.1038/35050073>.
- Yuan, X., Sobolev, S.V., Kind, R., 2002. Moho topography in the central Andes and its geodynamic implications. *Earth and Planetary Science Letters* 199, 389–402.